

# A model for the operation of perovskite based hybrid solar cells: formulation, analysis and comparison to experiment

J. M. Foster ‡\*    H. J. Snaith†    T. Leijtens†    G. Richardson\*.

August 24, 2016

## Abstract

This work is concerned with the modelling of perovskite based hybrid solar cells formed by sandwiching a slab of organic lead halide perovskite ( $\text{CH}_3\text{NH}_3\text{PbI}_{3-x}\text{Cl}_x$ ) photo-absorber between (n-type) acceptor and (p-type) donor materials - typically titanium dioxide and spiro. A model for the electrical behaviour of these cells is formulated based on drift-diffusion equations for the motion of the charge carriers and Poisson's equation for the electric potential. It is closed by (i) internal interface conditions accounting for charge recombination/generation and jumps in charge carrier densities arising from differences in the electron affinity/ionisation potential between the materials (ii) Ohmic boundary conditions on the contacts. The model is analysed by using a combination of asymptotic and numerical techniques. This leads to an approximate - yet highly accurate - expression for the current-voltage relationship as a function of the solar induced photo-current. In addition, we show that this approximate current-voltage relation can be interpreted as an equivalent circuit model consisting of three diodes, a resistor and a current source. For sufficiently small biases the device's behaviour is diodic and the current is limited by the recombination at the internal interfaces, whereas, for sufficiently large biases the device acts like a resistor and the current is dictated by the Ohmic dissipation in the acceptor and donor. The results of the model are also compared to experimental current-voltage curves and good agreement is shown.

---

\*School of Mathematics, University of Southampton, Southampton, SO17 1BJ, UK (jamie.michael.foster@gmail.com, g.richardson@soton.ac.uk). ‡Current address: Department of Mathematics and Statistics, McMaster University, Hamilton, L8S 4K1. Canada.

†Clarendon Laboratory, University of Oxford, Parks Road, Oxford, OX1 3PU, UK.

# 1 Introduction

Solar technology has been a very active field of research for many years. For the majority of this time the best cells have been made from inorganic crystalline semiconductors; with commercially available silicon modules typically operating in the range of 16-20% power conversion efficiency (PCE) [15]. However, during this time, the cost of their manufacture (in both a financial and environmental sense) has remained relatively high. More recently, a different class of solar cells has emerged that are manufactured using organic semiconductors. These organic devices present several important advantages over their traditional inorganic counterparts; for example, low cost materials, high throughput manufacturing techniques (e.g. roll-to-roll printing) and mechanical flexibility (allowing the placement of cells in previously unusable positions). Despite these advantages, the current organic devices have been unable to compete in the commercial market due to their relatively low efficiency. Until this year the best organic cells had around a 7-10% PCE [14, 15].

However, in only the last year, it has been discovered that hybrid organic cells constructed with a light-absorbing layer of perovskite can lead to a significant improvement in PCE [12, 21, 27]. This perovskite material acts as both a light absorber and an ambipolar charge (or exciton) transporting material, negating the need for nano-structured heterojunctions such as those used in most organic photovoltaics. Indeed, when this perovskite material is used in a thin film architecture, and a flat perovskite layer is placed between a titanium dioxide acceptor and a spiro donor, device performances of up to 15% PCE have been achieved [2, 43]. However, since the technology is new, and the underlying physics is not yet fully understood, it is anticipated that an even higher PCE is obtainable with the correct optimisation leading to a cell that is both cheap *and* operating at the highest efficiency.

In perovskite cells, absorption of light occurs mainly in the perovskite layer. Following light absorption there is a coexistence of excitons and free charges, owing to the exciton binding energy being on the order of the thermal energy ( $\sim 50$  meV) [26]. The exact branching ratio for excitons versus free charges remains unknown, and for the work presented here we assume that free charge generation is the predominant pathway. These free charges migrate through the perovskite by a combination of thermally excited diffusion and electrically induced drift. Selective flow of charges to the contacts is facilitated by the acceptor and donor layers abutting the perovskite, that act as a barrier to holes and electrons, respectively. There is evidence to suggest that efficient solar cell operation is aided by significant levels of n-doping in the acceptor ( $\sim 10^{22} - 10^{23}/\text{m}^3$ ) and p-doping in the donor ( $\sim 10^{23} - 10^{24}/\text{m}^3$ ) [37]. Charge (electron-hole) recombination can take place within the bulk of the perovskite and in narrow layers ( $\sim 1\text{nm}$ ) near the material interfaces.

Our approach to describing the electrical properties of a perovskite cell is (in §2) to for-

ulate a model based on: (i) drift-diffusion equations for the two species of charge carriers (hole and electrons) throughout the device and (ii) a version of Poisson's equation that accounts for doping in both the acceptor and donor. The effect of (iii) charge recombination is modelled near the material interfaces by appropriate internal boundary conditions and (iv) in the bulk of the perovskite by a bulk recombination term. Charge pair generation is modelled by (v) a bulk generation term within the perovskite while changes in electron affinity and ionisation potential at the material interfaces are systematically accounted for by (vi) jump conditions on the carrier densities at the material interfaces (see for example [33]). Finally (vii) Ohmic boundary conditions are prescribed on the contacts on the outer edges of the cell.

The model is analysed using a combination of asymptotic and numerical techniques. In the physically relevant regime, under illumination of one sun: (I) the Debye lengths in donor, perovskite and acceptor are all small in comparison to the width of the materials; (II) the charge mobilities in the perovskite are very much greater than those in the acceptor and donor; and (III) recombination is difficult - corresponding to small values of the dimensionless parameters  $\delta$ ,  $\delta K_l$  and  $\delta K_r$ , as defined later in (21). We note that if recombination were not difficult the device would behave primarily as an Ohmic resistor and it would not be possible to achieve the open-circuit voltages (of around 1 Volt) that are observed in real devices.

In practice, a combination of the properties (I) and (III) makes solution of the problem using numerical methods very challenging. Our approach, in §3, has been to use a numerical scheme to compute solutions in which the dimensionless Debye lengths are moderately small, and recombination is moderately difficult. However we are unable to solve for the extremely small dimensionless Debye lengths and values of  $\delta K_l$  and  $\delta K_r$  that occur in practice - a more detailed explanation of why this difficulty occurs is given in §3.

This motivated us, in §4, to adopt an asymptotic approach to the solution of the problem that systematically exploits the small dimensionless Debye lengths and large relative mobility in the perovskite (properties (I) and (II)) - previous authors have treated related, but different, problems using these techniques [1, 4, 8, 18, 30, 35, 38]. The resulting asymptotic solution compares very favourably to the full numerical solution in the appropriate regime (see figure 3). It also leads to a relatively simple set of transcendental equations for the current-voltage curve, which in the case of bimolecular recombination (§4.2) can be solved exactly. For certain types of non-bimolecular (§4.3) recombination the problem for the current-voltage curve can be reduced to the solution of a single algebraic equation. In §5 we compare experimental current-voltage curves to those predicted by the asymptotic solution to the model. Finally, in §6, we draw our conclusions.

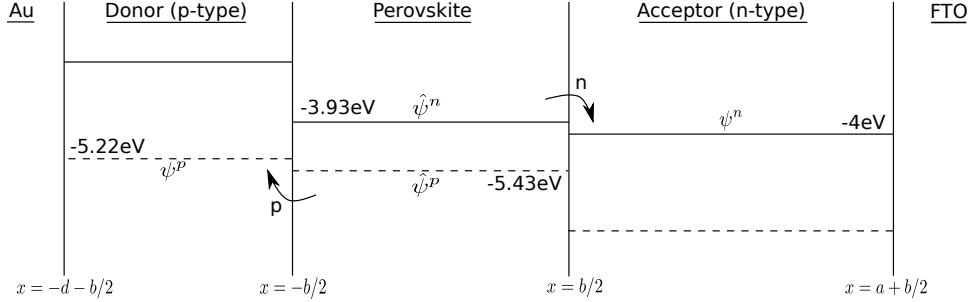


Figure 1: A sketch of a perovskite cell showing the HOMO/valence bands (dashed lines) and LUMO/conduction bands (solid lines).

## 2 Problem formulation

A sketch of the idealised geometry of a perovskite solar cell is given in figure 1; it consists of a p-type donor layer in  $-d - b/2 < x < -b/2$ , a perovskite layer in  $-b/2 < x < b/2$  and an n-type acceptor layer  $b/2 < x < a + b/2$ . The perovskite has a highly ordered crystalline structure which is associated with well-defined conduction and valence band edges separated by a band-gap. In contrast the organic acceptor and donor materials are amorphous and have no well-defined band structure. Electrons are excited into the lowest unoccupied molecular orbital (LUMO) leaving a hole in the highest occupied molecular orbital (HOMO) and conduction takes place as excited electrons and holes move between LUMO and HOMO (respectively) on adjacent molecules. This process is often viewed as a *hopping* process between shallow, highly localised, energy wells (termed ‘traps’) and a variety of different charge transport models are used to describe it including multiple trapping models [20], Gaussian disorder models [31], and atomistic models [24]. Nevertheless drift diffusion models are still widely used [5, 6, 9, 10, 16] to describe transport processes in organic semiconductors and indeed solutions of hopping models using Dynamic Monte-Carlo methods have been used to derive drift-diffusion parameters from microscopic data [22, 42]. Here we also opt to use a drift-diffusion description of the acceptor and donor materials and note that (from a mathematical view point) the energy level of the LUMO plays a role identical to that of the conduction band edge while that of the HOMO plays a role identical to that of the valence band edge. We denote the energy of an electron at the lower edge of the conduction band (or LUMO) by  $E_c(x)$ , and that of a hole at the upper edge of the valence band (or HOMO) by  $E_v(x)$ . These quantities can be conveniently split into material dependent parts ( $\bar{\mu}^n(x)$  and  $\bar{\mu}^p(x)$ ) and parts arising from electrostatic interactions

so that they can be written in the form

$$E_c(x) = \bar{\mu}^n(x) - q\phi \quad \text{and} \quad E_v(x) = \bar{\mu}^p(x) - q\phi, \quad (1)$$

where,  $\phi$  is the electric potential and  $q$  is the elementary charge. The material properties  $\bar{\mu}^n(x)$  and  $\bar{\mu}^p(x)$  are the electron affinity and ionization potential respectively, which, in this problem, are piece-wise constant functions that can be written as

$$\bar{\mu}^n(x) = \begin{cases} \hat{\mu}^n & \text{for } -b/2 < x < b/2, \\ \mu^n & \text{for } b/2 < x < a + b/2, \end{cases} \quad (2)$$

$$\bar{\mu}^p(x) = \begin{cases} \mu^p & \text{for } -d - b/2 < x < -b/2, \\ \hat{\mu}^p & \text{for } -b/2 < x < b/2. \end{cases} \quad (3)$$

The ‘average’ force exerted on an electron in the conduction band (or LUMO) is thus  $-\nabla E_c$  while that exerted on a hole in the valence band (or HOMO)  $\nabla E_v$ . Notably the infinite gradients in  $\bar{\mu}^n$  and  $\bar{\mu}^p$  that occur at the interfaces between materials lead to effective discontinuities in the electron and hole concentrations. In practice these energy differences are so large that the hole concentration in the acceptor and the electron concentration in the donor are vanishingly small which is an important factor in limiting (undesirable) recombination of charge carriers in these materials. Henceforth we assume that  $\bar{\mu}^n$  and  $\bar{\mu}^p$  are constant within a material so that, with the exception of material interfaces, we can ignore forces arising from gradients in these quantities.

**Bulk equations** Charge carrier transport is modelled using drift-diffusion equations. In the donor, we assume that the electron concentration is zero (justified by the large jump in electron affinity between donor and perovskite) while in the acceptor we assume that the hole concentration is zero (justified by the large jump in ionization potential between acceptor and perovskite). The appropriate hole (electron) conservation equations in the donor (acceptor) are thus

$$q \frac{\partial p}{\partial t} + \frac{\partial J^p}{\partial x} = 0 \quad \text{where} \quad J^p = -qD_d \left( \frac{\partial p}{\partial x} + \frac{qp}{kT} \frac{\partial \phi}{\partial x} \right) \quad \text{in} \quad -(b/2 + d) < x < -b/2, \quad (4)$$

$$q \frac{\partial n}{\partial t} - \frac{\partial J^n}{\partial x} = 0 \quad \text{where} \quad J^n = qD_a \left( \frac{\partial n}{\partial x} - \frac{qn}{kT} \frac{\partial \phi}{\partial x} \right) \quad \text{in} \quad b/2 < x < b/2 + a. \quad (5)$$

where  $t$  denotes time,  $n$  and  $p$  are electron and hole number densities respectively,  $J^p$  and  $J^n$  are the hole and electron current densities respectively,  $D_d$  and  $D_a$  are the diffusivities

of a hole in the donor and an electron in the acceptor respectively,  $k$  is Boltzmann's constant and  $T$  is the absolute temperature.

In the perovskite both holes and electrons are created in abundance by photo-absorption which we model as a bulk generation term  $G(x)$  in the electron and hole conservation equations. We also incorporate terms, accounting for bulk recombination  $R(n, p)$  and thermal generation  $\mathcal{G}_t(n, p)$  of electron-hole pairs, into the conservation equations so that they take the form

$$\frac{\partial p}{\partial t} + \frac{1}{q} \frac{\partial J^p}{\partial x} = G - R(n, p) + \mathcal{G}_t(n, p), \quad \text{and} \quad J^p = -q \hat{D}_p \left( \frac{\partial p}{\partial x} + \frac{qp}{kT} \frac{\partial \phi}{\partial x} \right), \quad (6)$$

$$\frac{\partial n}{\partial t} - \frac{1}{q} \frac{\partial J^n}{\partial x} = G - R(n, p) + \mathcal{G}_t(n, p), \quad \text{and} \quad J^n = q \hat{D}_n \left( \frac{\partial n}{\partial x} - \frac{qn}{kT} \frac{\partial \phi}{\partial x} \right), \quad (7)$$

in  $-b/2 < x < b/2$ . Here  $\hat{D}_p$  and  $\hat{D}_n$  are the diffusivities of holes and electrons in the perovskite, respectively. The exact forms of the bulk generation, bulk recombination and bulk thermal generation terms  $G(x)$ ,  $R(n, p)$  and  $\mathcal{G}_t(n, p)$  are discussed later in this section.

The charge carrier conservation equations (4)-(7) are coupled to Poisson's equation for the electric potential,  $\phi$ , which takes the form

$$\frac{\partial^2 \phi}{\partial x^2} = \begin{cases} \frac{q}{\varepsilon_d} (\hat{N}_d - p) & \text{in } -(b/2 + d) < x < -b/2, \\ \frac{q}{\varepsilon_p} (n - p) & \text{in } -b/2 < x < b/2, \\ \frac{q}{\varepsilon_a} (n - \hat{N}_a) & \text{in } b/2 < x < b/2 + a, \end{cases} \quad (8)$$

where we incorporate the effect of doping, in the donor and acceptor, by including the terms  $\hat{N}_d$  and  $\hat{N}_a$ . Here  $\varepsilon_d$ ,  $\varepsilon_p$  and  $\varepsilon_a$  are the permittivities of the donor, perovskite and acceptor, respectively.

**Jump conditions at the material interfaces** Continuity of potential and electric displacement at the donor-perovskite interfaces and at the perovskite-acceptor interface take the form

$$\phi|_{x=-b/2^-} = \phi|_{x=-b/2^+}, \quad \varepsilon_d \phi_x|_{x=-b/2^-} = \varepsilon_p \phi_x|_{x=b/2^+}, \quad (9)$$

$$\phi|_{x=b/2^-} = \phi|_{x=b/2^+}, \quad \varepsilon_p \phi_x|_{x=b/2^-} = \varepsilon_a \phi_x|_{x=b/2^+}. \quad (10)$$

Continuity of electric current across the interfaces and electron-hole interface recombination conditions can be formulated as follows:

$$J^p|_{x=-b/2^-} = J^n + J^p|_{x=-b/2^+}, \quad J^n|_{x=-b/2^+} = qR_l(n, p) - q\mathcal{G}_{lt}(n, p), \quad (11)$$

$$J^n|_{x=b/2^-} + J^p|_{x=b/2^-} = J^n|_{x=b/2^+}, \quad J^p|_{x=b/2^-} = qR_r(n, p) - q\mathcal{G}_{rt}(n, p), \quad (12)$$

where  $R_l$  and  $R_r$  are the electron-hole recombination rates on the donor-perovskite and perovskite-acceptor interfaces respectively,  $\mathcal{G}_{lt}$  and  $\mathcal{G}_{rt}$  are the rates of thermal generation of electron-hole pairs on the donor-perovskite and perovskite-acceptor interfaces respectively. Here, as is usual, we assume that there is no net surface charge on the semiconductor-semiconductor interfaces. We note however that these interfaces can be populated by a high density of traps so it is possible to envisage situations where large charge densities reside on the surfaces, but we do not consider this scenario here. The ratio of the hole concentrations (on either side of the donor-perovskite interface) and of the electron concentrations (on either side of the perovskite-acceptor interface) are given in terms of the jumps in the ionization potential and electron affinity (see, for example, [33]) by

$$p|_{x=-b/2^+} = \nu_p p|_{x=-b/2^-} \quad \text{where} \quad \nu_p = \frac{\hat{g}_v}{g_v} \exp\left(\frac{\hat{\mu}^p - \mu^p}{kT}\right), \quad (13)$$

$$n|_{x=b/2^-} = \nu_n n|_{x=b/2^+} \quad \text{where} \quad \nu_n = \frac{\hat{g}_c}{g_c} \exp\left(-\frac{\hat{\mu}^n - \mu^n}{kT}\right). \quad (14)$$

where  $g_c$  and  $\hat{g}_c$  are the conduction band density of states in the acceptor and perovskite, respectively, and  $g_v$  and  $\hat{g}_v$  are the valence band density of states in the donor and perovskite, respectively. Further details on the derivation of the conditions (13) and (14) are given in §A.

**Choice of bulk and surface recombination rates** The exact recombination mechanisms (both surface and bulk) in perovskite cells are still not yet well understood. However, since the perovskite has a well defined crystalline structure it is reasonable to assume that bulk recombination occurs directly and is thus bimolecular (*i.e.* has the form  $R \propto np$ ). Bimolecular recombination is associated with diodic behaviour with ideality factor  $\mathcal{N} = 1$ . In contrast, there is experimental evidence to suggest that the recombination at the material interfaces occurs via intermediate trap states so that a more general recombination condition, of the form  $R_{l,t} \propto n^\alpha p^\beta$ , is appropriate [23]. This form of the recombination is associated with diodic behaviour with ideality factor  $\mathcal{N} = 2/(\alpha + \beta)$ .

The requirement that the system has a genuine equilibrium in the dark (where the applied voltage and *all* current flows are zero) is tantamount to imposing that  $R - \mathcal{G}_t$ ,  $R_l - \mathcal{G}_{lt}$  and  $R_r - \mathcal{G}_{rt}$  all have the form  $\Gamma(n, p)(np - N_D^2)$  for some functions  $\Gamma(n, p)$  where  $n$ ,  $p$  and  $N_D$  are the electron, hole and intrinsic carrier densities in the perovskite ( $N_D$  is defined in terms of fundamental material properties in (131)). Even with these requirements there is still scope to model different recombination mechanisms through the choice of the functions  $\Gamma(n, p)$  in the three recombination conditions. Here, we initially model both bulk and surface recombinations using Langevin conditions, corresponding to direct recombination

of electron-hole pairs, by writing

$$R - \mathcal{G}_t = \hat{K}(np - N_D^2), \quad R_l - \mathcal{G}_{lt} = \hat{K}_l(np - N_D^2), \quad R_r - \mathcal{G}_{rt} = \hat{K}_r(np - N_D^2), \quad (15)$$

where  $\hat{K}$ ,  $\hat{K}_l$  and  $\hat{K}_r$  are constants. We note that this choice of recombination conditions inherently leads to an ideality factor  $\mathcal{N} = 1$ . Later, in §4.3 we treat a much broader class of recombination conditions, which can model a general ideality factor, and discuss how these alterations affect the predictions of the model.

**Boundary conditions at the contacts** The problem is closed by imposing Ohmic boundary conditions at the contacts with the electrodes. This is tantamount to assuming that there are sufficient surface recombination sites, so as to ensure that local equilibrium is always maintained, and that tunnelling effects at the contacts (and the diode-like behaviour) can be neglected<sup>1</sup>. In order that the model has a genuine equilibrium in the dark, in which the applied voltage and all current flows are zero, it is a requirement that the global condition (133) is satisfied (derived in §A). This can be ensured by writing the Ohmic boundary conditions in the form

$$p|_{x=-(b/2+d)} = \frac{N_D}{\tilde{N}_- \sqrt{\nu_n \nu_p}} \exp\left(\frac{qV_{bi}}{2kT}\right) \quad (16)$$

$$n|_{x=b/2+a} = \frac{\tilde{N}_- N_D}{\sqrt{\nu_n \nu_p}} \exp\left(\frac{qV_{bi}}{2kT}\right), \quad (17)$$

$$\phi|_{x=-(b/2+d)} = V_l - \frac{V_{bi}}{2}, \quad \phi|_{x=b/2+a} = -V_r + \frac{V_{bi}}{2}, \quad (18)$$

where  $V = V_l + V_r$  is the applied voltage and  $V_{bi}$  is the built in potential across the whole device (as defined in (128)). In terms of the fundamental material properties of the device (as discussed in §A)

$$\tilde{N}_- = \sqrt{\frac{g_c}{g_v}} \exp\left(-\frac{\mu_p + \mu_n + W_{cath} + W_{anod}}{2kT}\right).$$

In non-steady state the currents measured at the two contacts (i.e.  $J|_{x=-(b/2+d)}$  and  $J|_{x=b/2+a}$ ) will, in general, be different. In order to determine the *single* current flowing in the external circuit one must account for the rate of change of the surface charge densities at the metal contacts. However, this is not a problem at steady state where the currents on at the

---

<sup>1</sup>If tunnelling effects at the contacts were believed to be significant one could, for example, incorporate the conditions introduced by Malliaras and Scott, see [29]



two contacts must be identical and equal to that flowing in the external circuit. Finally, for convenience, we choose an origin for the electric potential in the middle of the perovskite material

$$\phi|_{x=0} = 0, \quad (19)$$

such that  $V_l$  and  $V_r$  are the potential differences across the left- and right-hand sides of the device respectively.

## 2.1 Non-dimensionalisation

Here we introduce dimensionless variables (denoted by a star) by scaling the model variables appropriately. We scale space with the width of the perovskite layer, voltages with the thermal voltage and current densities with the typical photo-generated current density  $qG_0b$  (where  $G_0$  is a typical value of  $G$  - the rate of photo-generation of charge pairs per unit volume). Carrier charge densities are scaled with  $\Pi_0 = b^2G_0/\sqrt{D_aD_d}$ , the typical charge density required to carry a current of magnitude  $qG_0b$ . The appropriate scalings thus takes the form

$$\begin{aligned} x &= bx^*, & p &= \Pi_0 p^*, & n &= \Pi_0 n^*, & \phi &= \frac{kT}{q} \phi^*, & G &= G_0 G^*, \\ \mathcal{G}_t &= G_0 \mathcal{G}_t^*, & \mathcal{G}_{lt} &= bG_0 \mathcal{G}_{lt}^*, & \mathcal{G}_{rt} &= bG_0 \mathcal{G}_{rt}^*, & R &= G_0 R^*, & R_l &= bG_0 R_l^*, \\ R_r &= bG_0 R_r^*, & J &= qG_0 b J^*, & J^n &= qG_0 b J^{n*}, & J^p &= qG_0 b J^{p*}, & V_{bi} &= \frac{kT}{q} \Phi_{bi}^*, \\ V_l &= \frac{kT}{q} \Phi_l^*, & V_r &= \frac{kT}{q} \Phi_r^*, & t &= \frac{b^2}{\sqrt{D_a D_d}} t^*, \end{aligned} \quad (20)$$

and gives rise to the following dimensionless quantities that characterise the system:

$$\begin{aligned} \Lambda_d &= \sqrt{\frac{\varepsilon_d}{\varepsilon_p}}, & \Lambda_a &= \sqrt{\frac{\varepsilon_a}{\varepsilon_p}}, & \kappa &= \sqrt{\frac{D_d}{D_a}}, & \kappa_n &= \frac{\hat{D}_n}{\sqrt{D_a D_d}}, & \kappa_p &= \frac{\hat{D}_p}{\sqrt{D_a D_d}}, \\ \delta &= \frac{\hat{K} \Pi_0^2}{G_0}, & w_d &= \frac{d}{b}, & w_a &= \frac{a}{b}, & N_a &= \frac{\hat{N}_a}{\Pi_0}, & N_d &= \frac{\hat{N}_d}{\Pi_0}, \\ N &= \frac{N_D}{\Pi_0}, & K_l &= \frac{\hat{K}_l}{\hat{K} b}, & K_r &= \frac{\hat{K}_r}{\hat{K} b}, & \lambda &= \sqrt{\frac{\varepsilon_p kT}{q^2 b^2 \Pi_0}}, & \nu_p &= \frac{\hat{g}_v}{g_v} \exp\left(\frac{\hat{\mu}^p - \mu^p}{kT}\right), \\ & & & & & & & & \nu_n &= \frac{\hat{g}_c}{g_c} \exp\left(-\frac{\hat{\mu}^n - \mu^n}{kT}\right). \end{aligned} \quad (21)$$

Of the parameters whose meaning is not self-evident from their definition:  $\nu_n$  is the ratio of the electron concentration in the perovskite to that in the acceptor adjacent to the perovskite-acceptor boundary;  $\nu_p$  is the ratio of the hole concentration in the perovskite to that in the donor adjacent to the perovskite-donor boundary;  $\lambda$  is the ratio of the Debye length in the perovskite to the width of the perovskite layer;  $\lambda\Lambda_a$  is the ratio of the Debye length in the acceptor to the width of the perovskite layer;  $\lambda\Lambda_d$  is the ratio of the Debye length in the donor to the width of the perovskite layer; and  $\delta$  is ratio of the typical bulk recombination to the typical bulk generation in the perovskite.

**The Steady Dimensionless Equations** Since our primary focus here is to derive expressions for the current-voltage relation of the cell we consider only the steady state, in which the total current throughout the device is a constant,  $J$ ; this can be seen by integrating (4a), (5a) and the difference between (6) and (7) and imposing continuity of current (11a) and (12a)). On applying the rescalings (20) to the steady-state version of the model (4)-(19) and dropping the stars we retrieve the dimensionless steady-state problem

$$\left. \begin{aligned} J &= -\kappa(p_x + p\phi_x) \\ \Lambda_d^2 \phi_{xx} &= \frac{1}{\lambda^2}(N_d - p) \end{aligned} \right\} \text{in } -w_d - \frac{1}{2} < x < -\frac{1}{2}, \quad (22)$$

$$\left. \begin{aligned} J_x^p &= G - \delta(np - N^2) \\ J_x^n &= \delta(np - N^2) - G \\ J^p &= -\kappa_p(p_x + p\phi_x) \\ J^n &= \kappa_n(n_x - n\phi_x) \\ \phi_{xx} &= \frac{1}{\lambda^2}(n - p) \end{aligned} \right\} \text{in } -\frac{1}{2} < x < \frac{1}{2}, \quad (23)$$

$$\left. \begin{aligned} J &= \frac{1}{\kappa}(n_x - n\phi_x) \\ \Lambda_a^2 \phi_{xx} &= \frac{1}{\lambda^2}(n - N_a) \end{aligned} \right\} \text{in } \frac{1}{2} < x < \frac{1}{2} + w_a, \quad (24)$$

subject to the jump conditions

$$\left. \begin{array}{l} \nu_p p_- = p_+ \quad \Lambda_d^2 \phi_x|_- = \phi_x|_+ \quad \phi_- = \phi_+ \\ J_+^n + J_+^p = J \quad J_+^n = K_l \delta(n_+ p_+ - N^2) \end{array} \right\} \text{ across } x = -\frac{1}{2}, \quad (25)$$

$$\left. \begin{array}{l} n_- = \nu_n n_+ \quad \phi_x|_- = \Lambda_a^2 \phi_x|_+ \quad \phi_- = \phi_+ \\ J_-^n + J_-^p = J \quad J_-^p = K_r \delta(n_- p_- - N^2) \end{array} \right\} \text{ across } x = \frac{1}{2}, \quad (26)$$

(where subscripts  $-$  and  $+$  denote quantities evaluated just to the left and just to the right of the interface respectively) and the boundary conditions

$$\left. \begin{array}{l} p = \frac{N}{\tilde{N}_- \sqrt{\nu_n \nu_p}} \exp\left(\frac{\Phi_{bi}}{2}\right) \\ \phi = -\frac{\Phi_{bi}}{2} + \Phi_l \end{array} \right\} \text{ on } x = -w_d - \frac{1}{2}, \quad (27)$$

$$\left. \begin{array}{l} n = \frac{N \tilde{N}_-}{\sqrt{\nu_n \nu_p}} \exp\left(\frac{\Phi_{bi}}{2}\right) \\ \phi = \frac{\Phi_{bi}}{2} - \Phi_r \end{array} \right\} \text{ on } x = \frac{1}{2} + w_a, \quad (28)$$

$$\left. \begin{array}{l} \phi = 0 \end{array} \right\} \text{ on } x = 0, \quad (29)$$

Here we can either choose to: (i) specify  $J$ , and use the solution to the problem to obtain  $\Phi_l$ ,  $\Phi_r$  and in turn the dimensionless applied potential  $\Phi = \Phi_l + \Phi_r$  or; (ii) specify the dimensionless applied potential  $\Phi = \Phi_l + \Phi_r$  and use the solution to the problem to obtain  $J$ . We note further that we can eliminate  $J^p$  from the problem by adding (23a) to (23b), integrating and applying the jump conditions (25c) and (26c) to obtain

$$J^p = J - J^n, \quad (30)$$

and henceforth we replace  $J^p$  by this expression.

### 2.1.1 Parameter estimates for real devices

Here we use existing data to obtain estimates for the sizes of the dimensionless parameters. We will base our calculations on a cell constructed using a  $\text{TiO}_2$  acceptor, a lead triiodide perovskite absorbing layer ( $\text{CH}_3\text{NH}_3\text{PbI}_3$ ) and a spiro-OMeTAD donor. A typical experimental current-voltage curve for this type of cell is shown in figure 5. We note that

other materials are also commonly used, for example, Lee *et al.* [27] investigated the performance of a methylammonium lead iodide chloride ( $\text{CH}_3\text{NH}_3\text{PbI}_{3-x}\text{Cl}_x$ ) perovskite cell and reported similar levels of performance. Parameter estimates for our system of choice are shown in table 1. The corresponding dimensionless parameter values are

$$\begin{aligned} \kappa &\approx 0.3162, & \hat{\kappa}_n = \hat{\kappa}_p &\approx 3.1623 \times 10^4, & \Lambda_d &\approx 0.7746, & \Lambda_a &\approx 4, \\ w_d &\approx 1.2, & w_a &\approx 0.2, & \nu_n &\approx 6.68 \times 10^{-2}, & \nu_p &\approx 2.9874 \times 10^{-4}. \end{aligned} \quad (31)$$

We can also obtain estimates for  $G_0$ ,  $\Pi_0$  and  $\lambda$  based on the current-voltage curve plotted in figure 5 by observing that the reverse saturation current density  $J_{rev,sat} \approx -200$  A/m<sup>2</sup> is given to a reasonable approximation by  $-q \int_{-b/2}^{b/2} G dx$ . Assuming almost uniform generation through the perovskite and taking  $b$  from table 1 yields a typical value for the generation rate of  $G_0 \approx 2.5 \times 10^{27}$  /m<sup>3</sup>s. In turn this corresponds to  $\Pi_0 \approx 7.9 \times 10^{23}$  /m<sup>3</sup> (via  $\Pi_0 = b^2 G_0 / \sqrt{D_a D_d}$ ) and  $\lambda \approx 0.96 \times 10^{-2}$ . The value of  $N_D$ , the intrinsic carrier concentration in the perovskite  $\text{CH}_3\text{NH}_3\text{PbI}_{3-x}\text{Cl}_x$ , is as yet unknown. It is however expected to be much less than the typical carrier concentrations  $\Pi_0$  in the device under illumination. In silicon, for example  $N_D \approx 1.5 \times 10^{16}$  m<sup>-3</sup> [39] which would, if repeated in the perovskite, give a value for  $N \approx 2 \times 10^{-8}$ . In agreement with the discussion in §1 the dimensionless dopant concentrations,  $N_a$  and  $N_d$ , are expected to be approximately  $O(1)$ . The remaining dimensionless parameters in the model ( $\delta$ ,  $K_l$ ,  $K_r$ ,  $\tilde{N}_-$ ) are more difficult to estimate (even using the curve shown in figure 5) without first analysing the model in detail and are therefore taken to be  $O(1)$  quantities for the purposes of the ensuing analysis.

### 3 Numerics

Our approach to the numerical solution of the system of equations (22)-(30) is to make a series of transformations that pose all three parts of the problem on the interval  $(-1/2, 1/2)$ . In order to do this we make the following changes of variable:

$$\begin{aligned} x = -1/2 - w_d \left( z + \frac{1}{2} \right), & \quad p(x) = \hat{p}(z), \quad \phi(x) = \hat{\phi}(z), \quad J^p(x) = \hat{J}^p(z), & \text{in} & \quad -w_d - \frac{1}{2} < x < -\frac{1}{2}, \\ x = z, & & \text{in} & \quad -\frac{1}{2} < x < \frac{1}{2}, \\ x = 1/2 + w_a \left( \frac{1}{2} - z \right), & \quad n(x) = \tilde{n}(z), \quad \phi(x) = \tilde{\phi}(z), \quad J^n(x) = \tilde{J}^n(z) & \text{in} & \quad \frac{1}{2} < x < \frac{1}{2} + w_a. \end{aligned} \quad (32)$$

Parameter	Symbol	Value	Reference(s)
Hole diffusivity in donor	$D_d$	$10^{-10}\text{m}^2/\text{s}$	[28]
Electron diffusivity in acceptor	$D_a$	$2.5 \times 10^{-9}\text{m}^2/\text{s}$	[28]
Electron diffusivity in perovskite	$\hat{D}_n$	$2.5 \times 10^{-5}\text{m}^2/\text{s}$	[37]
Hole diffusivity in perovskite	$\hat{D}_p$	$2.5 \times 10^{-5}\text{m}^2/\text{s}$	[37]
Donor permittivity	$\varepsilon_d$	$3\varepsilon_0\text{F/m}$	[37]
Acceptor permittivity	$\varepsilon_a$	$80\varepsilon_0\text{F/m}$	[37]
Perovskite permittivity	$\varepsilon_p$	$6.5\varepsilon_0\text{F/m}$	[37]
Acceptor width	$a$	50 – 100nm	[37]
Donor width	$d$	500 – 700nm	[37]
Perovskite width	$b$	500nm	[37]
Energy of LUMO in acceptor	$\mu_n$	-4eV	[12, 21]
Energy of HOMO in donor	$\mu_p$	-5.22eV	[21]
Energy of conduction band edge in perovskite	$\hat{\mu}_n$	-3.93eV	[12, 21]
Energy of valence band edge in perovskite	$\hat{\mu}_p$	-5.43eV	[12, 21]

Table 1: Parameter values for the device described in §2.1.1. Here,  $\varepsilon_0$  is the permittivity of free space.

By doing so we can transform the steady-state problem (22)-(30) to one on the domain  $-1/2 < z < 1/2$  formed by the eight equations

$$\begin{aligned}
w_d J &= \kappa \left( \hat{p}_z + \hat{p} \hat{\phi}_z \right), & \Lambda_d^2 \lambda^2 \hat{\phi}_{zz} &= w_d^2 (N_d - \hat{p}), & J_z^n + G &= \delta (np - N^2), \\
J - J^n &= -\hat{\kappa}_p (p_z + p \phi_z), & J^n &= \hat{\kappa}_n (n_z - n \phi_z), & \lambda^2 \phi_{zz} &= (n - p), \\
\kappa w_a J &= - \left( \tilde{n}_z - \tilde{n} \tilde{\phi}_z \right), & \Lambda_a^2 \lambda^2 \tilde{\phi}_{zz} &= w_a^2 (n - N_a).
\end{aligned} \tag{33}$$

and the thirteen boundary conditions

$$\left. \begin{aligned}
 \tilde{n} &= \frac{N\tilde{N}_-}{\sqrt{\nu_n\nu_p}} \exp\left(\frac{\Phi_{bi}}{2}\right) \\
 \tilde{\phi} &= \frac{\Phi_{bi}}{2} - \Phi_r \\
 p &= \nu_p\hat{p} \\
 \phi &= \hat{\phi} \\
 \frac{\partial\phi}{\partial z} &= -\frac{\Lambda_d^2}{w_d} \frac{\partial\hat{\phi}}{\partial z} \\
 J_n &= \delta K_l(np - N^2)
 \end{aligned} \right\} \text{ on } z = -\frac{1}{2},$$

$$\left. \begin{aligned}
 \hat{p} &= \frac{N}{\tilde{N}_-\sqrt{\nu_n\nu_p}} \exp\left(\frac{\Phi_{bi}}{2}\right) \\
 \hat{\phi} &= -\frac{\Phi_{bi}}{2} + \Phi_l \\
 n &= \nu_n\tilde{n} \\
 \phi &= \tilde{\phi} \\
 \frac{\partial\phi}{\partial z} &= -\frac{\Lambda_a^2}{w_a} \frac{\partial\tilde{\phi}}{\partial z} \\
 J - J_n &= \delta K_r(np - N^2)
 \end{aligned} \right\} \text{ on } z = \frac{1}{2}, \quad (34)$$

$$\phi|_{z=0} = 0. \quad (35)$$

The system (33)-(35) comprises an eleventh order set of ODEs with thirteen boundary conditions. Thus, on imposing  $J$  and leaving the two parameters  $\Phi_l$  and  $\Phi_r$  to be determined as part of the solution, it is not unreasonable to expect that (33)-(35) is well-posed. We solve (33)-(35) using the open source software ‘chebfun’ [11, 40], which approximates functions by Chebyshev polynomials, and is particularly appropriate for solving stiff problems. Nevertheless, this approach still has difficulty in solving the problem (33)-(35) with physically realistic parameter values and here we use it as a tool to gain insight into the behaviour of the problem for less extreme parameter values and to compare to our asymptotic analysis of the problem. The properties of the system that makes this a particularly challenging numerical problem are: (i) the small value of the dimensionless Debye length,  $\lambda$ , and; (ii) the small values of dimensionless recombination rate constants  $\delta K_l$  and  $\delta K_r$ . Inspecting the recombination boundary conditions in (34) one can see that the product  $np$  must become extremely large - specifically  $O(1/K_l\delta)$  or  $O(1/K_r\delta)$  - on the internal interfaces in order to reach the series resistance limited regime where  $J = O(1)$ . When these large values of the product  $np$  are reached, Poisson’s equation in (33) becomes extremely stiff owing to a combination of the small value of  $\lambda$  and the large values of  $n$  and  $p$ .

In figure 3 we show some representative current-voltage curves, potential profiles and charge carrier density profiles computed using this numerical scheme. A well-documented version of our code is provided in the supplementary material.

## 4 Asymptotic solution to the model in the limit of large perovskite conductivity and small Debye length

On estimating the model parameters from the data on real cells (see §2.1.1) it is apparent that there are very large disparities between hole and electron diffusivities in the perovskite and those in the donor and acceptor. The crystalline structure of the perovskite leads to a high electrical conductivity (corresponding to large electron and hole diffusivities) in comparison to the donor and acceptor which have much smaller conductivities (small electron and hole diffusivities). These properties manifest themselves in the dimensionless model in large values of  $\hat{\kappa}^p$  and  $\hat{\kappa}^n$  which are both  $O(10^4)$ . Physically we expect them to lead to a situation in which electron and hole densities rapidly equilibrate within the perovskite and in which the primary resistance to current flow is in the donor and acceptor layers. Moreover, we recall that  $\lambda$ , the ratio of the Debye length in the perovskite to the width of the perovskite layer, is small being of  $O(10^{-2})$  which results in approximate charge neutrality ( $n \approx p$ ) in the bulk of each material. The large difference in electron affinity between the acceptor (where it is high) and the perovskite (where it is low) mean that electron densities immediately adjacent to the perovskite-acceptor boundary are much greater in the acceptor than in the perovskite; this corresponds to a small value of dimensionless parameter  $\nu_n$  which is of  $O(10^{-2})$ . Analogously the large difference in ionization potential between the donor (where it is low) and the perovskite (where it is high) mean that hole densities immediately adjacent to the donor-perovskite boundary are much greater in the donor than in the perovskite corresponding to a small value of dimensionless parameter  $\nu_p$  which is of  $O(10^{-4})$ . From a physical perspective this can be interpreted as the acceptor and donor efficiently acting to ‘suck’ free-electrons and holes (respectively) out of the perovskite. Finally, since we are primarily interested in the operation of devices under illumination we expect the dimensionless thermal generation rate  $N \ll 1$ . However, it turns out that taking  $\nu_n$ ,  $\nu_p$  and  $N$  to be  $O(1)$  quantities results in a distinguished limit that is also valid, in the physical case, when  $\nu_n, \nu_p, N \ll 1$ . In order to make it clear that the asymptotic analysis does not rely on  $\nu_n$ ,  $\nu_p$  and  $N$  being small we therefore take them to be  $O(1)$  for the purposes of the ensuing analysis.

Motivated by these arguments we investigate the solution to the system (22)-(29) in the physically relevant asymptotic limit  $\hat{\kappa}^p = O(1/\lambda^2)$  and  $\hat{\kappa}^n = O(1/\lambda^2)$  where  $\lambda \ll 1$  (in the specific case discussed in §2.1.1  $\lambda = O(10^{-2})$ ). We formally take all other parameters to be of  $O(1)$ . In order to aid clarity, we re-express all large and small parameters in terms of  $O(1)$  over-barred variables by writing

$$\kappa_p = \frac{\bar{\kappa}_p}{\lambda^2} \quad \text{and} \quad \kappa_n = \frac{\bar{\kappa}_n}{\lambda^2}. \quad (36)$$

As we have defined the problem the power generating regime of the current-voltage curve lies in the quadrant  $J < 0$  and  $\Phi = \Phi_l + \Phi_r > 0$ . Since this is the section of the curve that is of most practical interest, in the remainder of this section, we focus on the current regime  $J < 0$ . Later, in §4.2 we discuss the cases  $J = 0$  and  $J > 0$ . It turns out that (in the small  $\lambda$  limit) the leading order solutions in the acceptor and donor region decouple from each other and since the solution structure in the donor and acceptor are very similar we only detail the solution derivation in the perovskite and acceptor layers and merely summarise the results for the donor. The relevant equations and boundary conditions in these two regions are obtained from (23), (24), (26), (28) and (29) and are

$$\left. \begin{aligned} p_x + p\phi_x &= \frac{\lambda^2}{\bar{\kappa}_p}(J^n - J), & J_x^n &= \delta(np - N^2) - G \\ n_x - n\phi_x &= \frac{\lambda^2}{\bar{\kappa}_n}J^n, & \phi_{xx} &= \frac{1}{\lambda^2}(n - p) \end{aligned} \right\} \text{ in } -\frac{1}{2} < x < \frac{1}{2}, \quad (37)$$

$$n_x - n\phi_x = \kappa J, \quad \phi_{xx} = \frac{1}{\Lambda_a^2 \lambda^2}(n - N_a) \quad \text{in } \frac{1}{2} < x < \frac{1}{2} + w_a, \quad (38)$$

$$\left. \begin{aligned} n|_{x=1/2^-} &= \nu_n n|_{x=1/2^+}, \\ \phi_x|_{x=1/2^-} &= \Lambda_a^2 \phi_x|_{x=1/2^+}, \\ \phi|_{x=1/2^-} &= \phi|_{x=1/2^+}, \\ (J^n - J)|_{x=1/2^-} &= -K_r \delta(n|_{x=1/2^-} p|_{x=1/2^-} - N^2) \end{aligned} \right\} \text{ across } x = \frac{1}{2} \quad (39)$$

$$n = \frac{N \tilde{N}_-}{\sqrt{\nu_n \nu_p}} \exp\left(\frac{\Phi_{bi}}{2}\right) \quad \text{and} \quad \phi = \frac{\Phi_{bi}}{2} - \Phi_r \quad \text{on } x = \frac{1}{2} + w_a, \quad (40)$$

$$\phi = 0 \quad \text{on } x = 0. \quad (41)$$

It also prove useful to recap the recombination condition

$$J_n|_{x=-1/2^+} = \delta K_l (n|_{x=-1/2^+} p|_{x=-1/2^+} - N^2). \quad (42)$$

#### 4.1 Matched asymptotic analysis with $J < 0$ in the limit $\lambda \rightarrow 0$

An asymptotic analysis of the problem in the limit  $\lambda \rightarrow 0$  requires that we split the device into seven regions, which we denote with the superscripts I-VII and depict in figure 2. These comprise the bulk regions (VI), (I) and (III) (in the donor, perovskite and acceptor, respectively), boundary layers about the donor-perovskite and perovskite-acceptor interfaces (regions (V) and (II), respectively) and boundary layers near the contact (regions (VII) and (IV)).



### 4.1.1 Features of the solution in the perovskite

Before proceeding with the matched asymptotic analysis we derive some general results that hold throughout the whole of the perovskite layer, whether in the bulk (I) or in the boundary layers (II) and (V). We note first (from (37a) and (37c)) that

$$p_x \sim -p\phi_x \quad \text{and} \quad n_x \sim n\phi_x, \quad (43)$$

in all three regions and it follows that the leading order behaviour of the solutions for  $n$  and  $p$  is given by

$$p \sim B \exp(-\phi) \quad \text{and} \quad n \sim A \exp(\phi) \quad \text{in} \quad -\frac{1}{2} < x < \frac{1}{2}, \quad (44)$$

for some, as yet undetermined, constants  $A$  and  $B$ . Taking these behaviours and substituting them in (37b) leads to the expression

$$J_x^n \sim \delta(AB - N^2) - G(x) \quad (45)$$

which can readily be integrated to give the leading order behaviour of the electron current throughout the perovskite

$$J^n \sim \delta(AB - N^2)x - \int_0^x G(s)ds + \frac{J}{2} - h \quad \text{in} \quad -\frac{1}{2} < x < \frac{1}{2} \quad (46)$$

for some constant  $h$  that remains to be determined. We can determine two relations for the unknown constants  $A$ ,  $B$  and  $h$  by substituting this expression for  $J^n$ , together with those for  $n$  and  $p$  found in (44), into the interface conditions (39d) and (42) to obtain

$$-\frac{\delta(AB - N^2) - J}{2} - h + \int_{-1/2}^0 G(x)dx \sim K_l \delta(AB - N^2), \quad (47)$$

$$-\frac{\delta(AB - N^2) - J}{2} + h + \int_0^{1/2} G(x)dx \sim K_r \delta(AB - N^2), \quad (48)$$

which we can solve to find expressions for  $h$  and  $AB$

$$\begin{aligned} h &= \frac{1}{2} \left[ \left( \frac{K_r - K_l}{K_l + K_r + 1} \right) \left( \int_{-1/2}^{1/2} G(x)dx + J \right) + \int_{-1/2}^0 G(x)dx - \int_0^{1/2} G(x)dx \right] \\ AB &= \frac{\int_{-1/2}^{1/2} G(x)dx + J}{\delta(K_l + K_r + 1)} + N^2. \end{aligned} \quad (50)$$

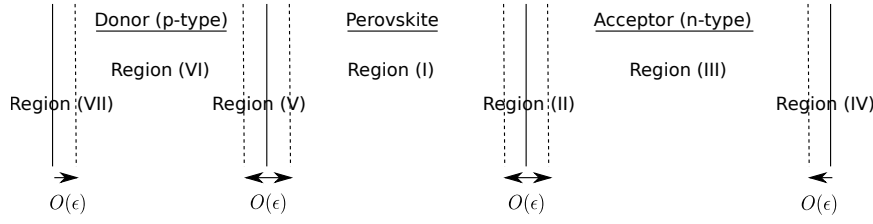


Figure 2: A sketch showing the locations and widths of the different asymptotic regions.

#### 4.1.2 The perovskite bulk: Region (I)

We begin by examining the solution in the perovskite bulk, away from the interfaces, by expanding in the form

$$n = n_0^{(I)} + O(\lambda^2), \quad p = p_0^{(I)} + O(\lambda^2) \quad \text{and} \quad \phi = \phi_0^{(I)} + O(\lambda^2). \quad (51)$$

Since  $\lambda \ll 1$ , the leading order balance in Poisson's equation, (37d), implies approximate charge neutrality,  $n_0^{(I)}(x) = p_0^{(I)}(x)$ . Then substitution of the expansion (51) into (37a) and (37c) yields

$$n_{0,x}^{(I)} + n_0^{(I)} \phi_{0,x}^{(I)} = 0, \quad n_{0,x}^{(I)} - n_0^{(I)} \phi_{0,x}^{(I)} = 0. \quad (52)$$

from which it follows that  $n_{0,x}^{(I)} = 0$  and  $\phi_{0,x}^{(I)} = 0$ . Applying the boundary condition (41), namely  $\phi_0^{(I)}|_{x=0} = 0$ , to the latter of these two equations and writing down a solution to the former that is compatible with (44) yields

$$n_0^{(I)} = A, \quad p_0^{(I)} = A \quad \text{and} \quad \phi_0^{(I)} = 0. \quad (53)$$

from which we see that  $B = A$ . It follows from (50) that

$$A = \sqrt{\frac{\int_{-1/2}^{1/2} G(x) dx + J}{\delta(K_l + K_r + 1)}} + N^2. \quad (54)$$

#### 4.1.3 The acceptor bulk: Region (III)

Having found the leading order solution in the perovskite bulk we look for a solution in the acceptor bulk. Once again the relatively small ratio of the Debye length to the width of the acceptor ( $\Lambda_a \lambda \ll 1$ ) gives rise to approximate charge neutrality throughout the bulk of the acceptor and motivates us to expand as follows:

$$n^{(III)} = n_0^{(III)} + O(\lambda^2) \quad \text{and} \quad \phi^{(III)} = \phi_0^{(III)} + O(\lambda^2). \quad (55)$$

Substituting this expansion into (38) and taking the leading order terms results in the following equations

$$n_{0,x}^{(III)} - n_0^{(III)} \phi_{0,x}^{(III)} = \kappa J \quad \text{and} \quad n_0^{(III)} = N_a. \quad (56)$$

Substituting the latter into the former and integrating with respect to  $x$  leads to the following relation for the leading order potential

$$\phi_0^{(III)} = -\frac{J\kappa}{N_a} \left( x - \frac{1}{2} \right) + c, \quad (57)$$

for some as yet undetermined constant  $c$ . From (57) it can be seen that the acceptor bulk is primarily behaving as an Ohmic resistor.

#### 4.1.4 Boundary layer about the acceptor-perovskite interface: Region (II)

We investigate the solution close to the perovskite-acceptor interface by rescaling distances in (37)-(39) as follows:

$$x = \frac{1}{2} + \lambda\eta. \quad (58)$$

This leads to following inner equations in the boundary layer:

$$\left. \begin{aligned} \phi_{\eta\eta} &= n - p \\ n_\eta - n\phi_\eta &= \lambda^3 \frac{J^n}{\bar{\kappa}_n} \\ p_\eta + p\phi_\eta &= \lambda^3 \frac{J^n - J}{\bar{\kappa}_p} \\ J_\eta^n &= \lambda(\delta(np - N^2) - G) \end{aligned} \right\} \quad \text{in } \eta < 0 \quad \text{and} \quad (59)$$

$$\left. \begin{aligned} \Lambda_a^2 \phi_{\eta\eta} &= n - N_a \\ n_\eta - n\phi_\eta &= \lambda J \kappa \end{aligned} \right\} \quad \text{in } \eta > 0, \quad (60)$$

respectively, which couple via the conditions

$$\left. \begin{aligned} n|_{\eta=0^-} &= \nu_n n|_{\eta=0^+}, \quad \phi_\eta|_{\eta=0^-} = \Lambda_a^2 \phi_\eta|_{\eta=0^+}, \\ \phi|_{\eta=0^-} &= \phi|_{\eta=0^+}. \end{aligned} \right\} \quad \text{across } \eta = 0. \quad (61)$$

We look for an asymptotic solution to (59)-(61) by expanding as follows:

$$n = n_0^{(II)} + O(\lambda^2), \quad p = p_0^{(II)} + O(\lambda^2) \quad \text{and} \quad \phi = \phi_0^{(II)} + O(\lambda^2). \quad (62)$$

We divide the task of looking for a solution to this problem by first solving in the perovskite, where  $\eta < 0$ , then solving in the acceptor, where  $\eta > 0$ , and finally ensuring appropriate continuity of the solution across the interface  $\eta = 0$  by applying the conditions (61).

**Solution in  $\eta < 0$  (the perovskite)** As discussed in §4.1.1 the leading order solutions for electron and hole densities in the perovskite have the form (44) corresponding to leading order solutions to (59b)-(59c) of the form

$$n_0^{(II)} = A \exp\left(\phi_0^{(II)}\right) \quad \text{and} \quad p_0^{(II)} = A \exp\left(-\phi_0^{(II)}\right) \quad \text{in} \quad \eta < 0, \quad (63)$$

where  $A$  is determined by (54). Substituting these solutions into the leading order expansion of (59a) results in the following Poisson-Boltzmann equation for the leading order potential

$$\phi_{0\eta\eta}^{(II)} = A \left( \exp\left(\phi_0^{(II)}\right) - \exp\left(-\phi_0^{(II)}\right) \right). \quad (64)$$

The far field behaviour of  $\phi^{(II)}$  is given by matching to region (I) in the limit  $\eta \rightarrow -\infty$  and is

$$\phi^{(II)} \rightarrow 0 \quad \text{as} \quad \eta \rightarrow -\infty. \quad (65)$$

Solutions to (64)-(65) have the form

$$\phi_0^{(II)} = \pm 2 \log \left[ \coth \left( \sqrt{\frac{A}{2}} (\eta_0 - \eta) \right) \right] \quad \text{in} \quad \eta < 0, \quad (66)$$

where  $\eta_0$  is a positive constant. Here we take the negative sign in this expression on the physical grounds that we know that - for all relevant operating conditions - the electron concentration is small in the perovskite in proximity to the boundary with acceptor, and is thus less than the hole concentration<sup>2</sup>. By substituting the leading order potential from (66) (on taking the negative sign) into the solution (63) we obtain the corresponding charge carrier densities

$$n_0^{(II)} = A \tanh^2 \left( \sqrt{\frac{A}{2}} (\eta_0 - \eta) \right) \quad \text{and} \quad p_0^{(II)} = A \tanh^{-2} \left( \sqrt{\frac{A}{2}} (\eta_0 - \eta) \right) \quad \text{in} \quad \eta < 0. \quad (67)$$

**Solution in  $\eta > 0$  (the acceptor)** The expansion of the drift-diffusion equation (60b) is, at leading order,

$$n_{0,\eta}^{(II)} - n_0^{(II)} \phi_{0,\eta}^{(II)} = 0 \quad \text{in} \quad \eta > 0, \quad (68)$$

---

<sup>2</sup>The only situation in which this is not the case, is when the device is operating very close to its reverse saturation current density and  $A \leq \nu_n N_a$ . However, we stress that this is not relevant in the interesting power-generating regime and so we do not pursue this further.

which has solution

$$n_0^{(II)} = M \exp\left(\phi_0^{(II)}\right) \quad \text{in } \eta > 0, \quad (69)$$

where  $M$  is a constant that remains to be determined.

**Matching to region (III) as  $\eta \rightarrow \infty$**  By matching to the leading order solution in the acceptor bulk (56)-(57) we obtain the following matching conditions on the leading order solution in region (II):

$$\phi_0^{(II)} \rightarrow c \quad \text{and} \quad n_0^{(II)} \rightarrow N_a \quad \text{as } \eta \rightarrow +\infty. \quad (70)$$

**Solution in  $\eta > 0$  (the acceptor) continued** The matching conditions (70) allows us to determine the unknown constant in (69) as  $M = N_a \exp(-c)$ . Then on substitution of (69) into the leading order expansion of Poisson's equation (60a) we obtain the following equation for the leading order potential  $\phi_0^{(II)}$ :

$$\Lambda_a^2 \phi_{0,\eta\eta}^{(II)} = N_a \left( \exp\left(\phi_0^{(II)} - c\right) - 1 \right). \quad (71)$$

By multiplying this equation by  $\phi_{0,\eta}^{(II)}$ , integrating with respect to  $\eta$ , applying the matching condition (70) and taking the negative square root of the results (thus ensuring that we are able to satisfy (61b) at leading order when we compare this solution in  $\eta > 0$  to (66)) we obtain the following expression for the derivative of the potential:

$$\Lambda_a \phi_{0,\eta}^{(II)} = -\sqrt{2N_a \left( \exp\left(\phi_0^{(II)} - c\right) - (\phi_0^{(II)} - c + 1) \right)}. \quad (72)$$

We can integrate this once more, this time with respect to  $\phi_0^{(II)}$ , in order to find an expression for  $\eta$  but, before doing so we enforce continuity of the potential across the interface  $\eta = 0$  through (61c), which, on noting that the solution in  $\eta < 0$  is given by (66), leads to the boundary condition

$$\phi_0^{(II)}|_{\eta=0^+} = -2 \log \left[ \coth \left( \sqrt{\frac{A}{2}} \eta_0 \right) \right]. \quad (73)$$

Integrating (72) and applying this boundary condition yields a parametric solution for the potential

$$\eta = \int_{\phi_0^{(II)}}^{-2 \log \left[ \coth \left( \sqrt{\frac{A}{2}} \eta_0 \right) \right]} \frac{\Lambda_a}{\sqrt{2N_a \left( \exp(s - c) - (s - c + 1) \right)}} ds \quad (74)$$

where  $\phi_0^{(II)} < -2 \log \left[ \coth \left( \sqrt{\frac{A}{2}} \eta_0 \right) \right]$ .

**Coupling the solution in  $\eta > 0$  to that in  $\eta < 0$  via the interface conditions** In order to determine the remaining constants in the solution, namely  $\eta_0$  and  $c$ , we impose the interface conditions (61a) and (61b). By substituting for  $n^{(II)}|_{\eta=0^-}$  (from (67)) for  $n_0^{(II)}|_{\eta=0^+}$  (from (69)) and for  $\phi_0^{(II)}|_{\eta=0}$  (from (73)) in (61a) we obtain an expression for  $c$ :

$$c = -\log\left(\frac{A}{\nu_n N_a}\right). \quad (75)$$

The remaining constant  $\eta_0$  is determined by substituting for  $\phi_{0,\eta}^{(II)}|_{\eta=0^-}$  (from the derivative of (66)) and for  $\phi_{0,\eta}^{(II)}|_{\eta=0^+}$  (from (72)-(73)) into (61b); this yields a transcendental equation for  $\eta_0$

$$\Lambda_a^2 N_a \sinh^2\left(\eta_0 \sqrt{2A}\right) \left[ \frac{A}{\nu_n N_a} \tanh^2\left(\eta_0 \sqrt{\frac{A}{2}}\right) - \log\left\{ \frac{A}{\nu_n N_a} \tanh^2\left(\eta_0 \sqrt{\frac{A}{2}}\right) \right\} - 1 \right] = 4A. \quad (76)$$

This is readily solved by using a numerical root-finding scheme.

#### 4.1.5 Near the acceptor contact: Region (IV)

To complete the description of the right-hand side of the device we study the behaviour near the acceptor contact where the charge carrier density must vary rapidly in order to satisfy the Ohmic boundary conditions. The structure of this boundary layer is similar to that in the acceptor near the internal interface (*i.e.*  $\eta > 0$  in §region II as discussed in the section above). We therefore suppress some of the details for brevity. We begin by performing the rescaling

$$x = \frac{1}{2} + w_a + \lambda \xi \quad (77)$$

in (38) and (40) so that the boundary layer equations and boundary conditions are

$$\Lambda_a^2 \phi_{\xi\xi}^{(IV)} = n^{(IV)} - N_a \quad \text{and} \quad n_{\xi}^{(IV)} - n^{(IV)} \phi_{\xi}^{(IV)} = -\lambda J_{\kappa} \quad \text{in} \quad \xi < 0, \quad (78)$$

$$\text{with} \quad \phi^{(IV)}|_{\xi=0} = \frac{\Phi_{bi}}{2} - \Phi_r \quad \text{and} \quad n^{(IV)}|_{\xi=0} = \frac{N \tilde{N}_-}{\sqrt{\nu_n \nu_p}} \exp\left(\frac{\Phi_{bi}}{2}\right). \quad (79)$$

Expanding as follows:

$$n^{(IV)} = n_0^{(IV)} + O(\lambda^2) \quad \text{and} \quad \phi^{(IV)} = \phi_0^{(IV)} + O(\lambda^2) \quad (80)$$

and matching to the solution in region (III), (56) and (57), leads to the following matching conditions on the leading order solution:

$$\phi_0^{(IV)} \rightarrow -w_a \frac{J\kappa}{N_a} + c \quad \text{and} \quad n_0^{(IV)} \rightarrow N_a \quad \text{as} \quad \xi \rightarrow -\infty. \quad (81)$$

The solution to the leading order expansion of (78b) that satisfies the matching conditions is

$$n_0^{(IV)} = N_a \exp \left( \phi_0^{(IV)} + w_a \frac{J\kappa}{N_a} - c \right). \quad (82)$$

Substituting this expression into the leading order expansion of (78a) and (79a) leads to the following:

$$\frac{\Lambda_a^2}{N_a} \phi_{0,\xi\xi}^{(IV)} = \left[ \exp \left( \phi_0^{(IV)} + w_a \frac{J\kappa}{N_a} - c \right) - 1 \right], \quad \phi_0^{(IV)}|_{\xi=0} = \frac{\Phi_{bi}}{2} - \Phi_r, \quad (83)$$

which, together with the matching condition (81a), has a parametric solution of the form

$$\xi = \pm \int_{\Phi_{bi}/2 - \Phi_r}^{\phi_0^{(IV)}} \frac{\Lambda_a}{\sqrt{2N_a \left( \exp \left( s + w_a \frac{J\kappa}{N_a} - c \right) - \left( s + w_a \frac{J\kappa}{N_a} - c + 1 \right) \right)}} ds, \quad (84)$$

where  $\xi < 0$ . Finally, we may determine  $\Phi_r$ , the potential drop across the right-hand side of the device (between  $x = 1/2 + w_a$  and  $x = 0$ ), by substituting for  $\phi^{(IV)}|_{\xi=0}$  (from (79a)),  $n_0^{(IV)}|_{\xi=0}$  (from (79b)) and for  $c$  (from (75)) in (82). We find that

$$\Phi_r = \log \left( \frac{A\sqrt{\nu_p}}{N\tilde{N}_-\sqrt{\nu_n}} \right) + \frac{w_a J\kappa}{N_a}. \quad (85)$$

#### 4.1.6 Solutions in the regions (V), (VI) and (VII)

The structure of the solution in the donor region is analogous to that in the acceptor. We therefore omit all detail of its derivation and give only the asymptotic expansions and the leading order solutions in each region.

**The donor bulk: (Region (VI))** Here the appropriate expansions for the potential and the hole density are

$$\phi^{(IV)} = \phi_0^{(VI)} + O(\lambda^2), \quad \text{and} \quad p^{(VI)} = p_0^{(VI)} + O(\lambda^2) \quad (86)$$

and the leading order solutions are

$$\phi_0^{(IV)} = -\frac{J}{\kappa N_d} \left( x + \frac{1}{2} \right) + \hat{c} \quad \text{and} \quad p_0^{(IV)} = N_d. \quad (87)$$

**The boundary layer about the donor-perovskite interface: Region (V)** Here we rescale about the interface by writing  $x = -1/2 + \lambda\chi$  and expand as follows:

$$\phi^{(V)} = \phi_0^{(V)} + O(\lambda^2), \quad n^{(V)} = n_0^{(V)} + O(\lambda^2), \quad p^{(V)} = p_0^{(V)} + O(\lambda^2). \quad (88)$$

In the perovskite where ( $\chi > 0$ ) the leading order solution is

$$\begin{aligned} n_0^{(V)} &= A \tanh^{-2} \left( \sqrt{\frac{A}{2}} (\chi + \chi_0) \right), & p_0^{(V)} &= A \tanh^2 \left( \sqrt{\frac{A}{2}} (\chi + \chi_0) \right), \\ \phi_0^{(V)} &= 2 \log \left[ \coth \left( \sqrt{\frac{A}{2}} (\chi + \chi_0) \right) \right], \end{aligned} \quad (89)$$

and in the donor ( $\chi < 0$ ) it has the form

$$p_0^{(V)} = N_d \exp \left( \hat{c} - \phi_0^{(V)} \right), \quad (90)$$

$$\chi = \int_{\phi_0^{(V)}}^{2 \log [\coth(\sqrt{\frac{A}{2}} \chi_0)]} \frac{\Lambda_d}{\sqrt{2N_d} ((s - \hat{c} - 1) + \exp(\hat{c} - s))} ds, \quad (91)$$

where the second equation is an implicit expression for  $\phi_0^{(V)}$ . Here the constant  $\hat{c}$  is given by

$$\hat{c} = \log \left( \frac{A}{\nu_p N_d} \right), \quad (92)$$

and the positive constant  $\chi_0$  is found by solving the transcendental equation

$$\Lambda_d^2 N_d \sinh^2 \left( \chi_0 \sqrt{2A} \right) \left[ \frac{A}{\nu_p N_d} \tanh^2 \left( \chi_0 \sqrt{\frac{A}{2}} \right) - \log \left\{ \frac{A}{\nu_p N_d} \tanh^2 \left( \chi_0 \sqrt{\frac{A}{2}} \right) \right\} - 1 \right] = 4A. \quad (93)$$

**The boundary layer about the donor contact: Region (VII)** Here we rescale about the contact by writing  $x = -(w_d + 1/2) + \lambda\omega$  and expand as follows:

$$\phi^{(VII)} = \phi_0^{(VII)} + O(\lambda^2), \quad p^{(VII)} = p_0^{(VII)} + O(\lambda^2). \quad (94)$$



The leading order solutions for the hole density and potential are given by the following explicit and implicit relations, respectively:

$$p_0^{(VII)} = N_d \exp \left( \hat{c} + \frac{Jw_d}{\kappa N_d} - \phi_0^{(VII)} \right), \quad (95)$$

$$\omega = \pm \int_{\Phi_l - \Phi_{bi}/2}^{\phi_0^{(VII)}} \frac{\Lambda_d}{\sqrt{2N_d \left( \left( s - \frac{Jw_d}{\kappa N_d} - \hat{c} - 1 \right) + \exp \left( \hat{c} + \frac{Jw_d}{\kappa N_d} - s \right) \right)}} ds. \quad (96)$$

Finally, the potential drop across across the left-hand side of the device (between  $x = 0$  and  $x = -1/2 - w_d$ ) can be determined as

$$\Phi_l = \log \left( \frac{\tilde{N}_- A \sqrt{\nu_n}}{N \sqrt{\nu_p}} \right) + \frac{Jw_d}{\kappa N_d}. \quad (97)$$

## 4.2 The current-voltage relation for bimolecular recombination ( $\mathcal{N} = 1$ )

In §4.1 we derived the asymptotic solution of (37)-(41), in the limit  $\lambda \rightarrow 0$ . This allows us to write an asymptotic expression for the current-voltage relation (between  $J$  and  $\Phi$ ), that is valid for all values of  $J$ , by (i) recalling that  $\Phi = \Phi_l + \Phi_r$ , (ii) substituting for  $\Phi_l$  using (97), and (iii) substituting for  $\Phi_r$  from (85). This takes the form

$$\Phi \sim \log \left( \frac{A^2}{N^2} \right) + J \left( \frac{w_d}{\kappa N_d} + \frac{w_a \kappa}{N_a} \right), \quad (98)$$

where  $A$  is, in the case of bimolecular recombination, given by (54). It follows that the current-voltage relation is

$$\Phi \sim \log \left( \frac{\int_{-1/2}^{1/2} G(x) dx + J}{N^2 \delta (K_l + K_r + 1)} + 1 \right) + J \left( \frac{w_d}{\kappa N_d} + \frac{w_a \kappa}{N_a} \right). \quad (99)$$

**Validity of asymptotics** It is clear that  $N$  is small but we have had, as yet, no way of estimating  $\delta$ . If we take the relation (99) and substitute  $J = 0$  we get an expression for the open circuit voltage  $\Phi_{oc}$  which we can invert to obtain an expression for  $\delta(K_l + K_r + 1)$

$$\delta(K_l + K_r + 1) \sim \frac{\int_{-1/2}^{1/2} G dx}{N^2 (\exp(\Phi_{oc}) - 1)}.$$

For a perovskite cell  $V_{oc} \approx 0.8\text{V}$  which equates to  $\Phi_{oc} \approx 32$ . Substituting for  $\delta(K_l + K_r + 1)$  in (54), from the above, we obtain, on neglecting small terms,

$$A \sim N \left[ \exp(\Phi_{oc}) \left( 1 + \frac{J}{\int_{-1/2}^{1/2} G(x) dx} \right) \right]^{1/2}. \quad (100)$$

It is required, in order for the asymptotics to be valid, that  $A/\lambda^2 \gg 1$ ; this ensures the existence of a Debye layer in the perovskite. Substituting  $N = 2 \times 10^{-8}$  (as estimated previously from silicon),  $\lambda = 10^{-2}$  and  $\Phi_{oc} = 32$  we see that the condition  $A/\lambda^2 \gg 1$  is satisfied for most of the current voltage curve but fails close to  $J_{sc}$ , the short-circuit current (where  $\Phi = 0$ ).

### 4.3 Extension to non-bimolecular recombination ( $\mathcal{N} \neq 1$ )

Here we investigate how alterations to the surface recombination rates affect the current-voltage curve. Physically, alterations may be appropriate if the recombination of charges across the interface between the donor-perovskite and perovskite-acceptor interfaces is trap mediated - that is, recombination occurs through intermediate trap states. In this case [23, 34] it has been argued that the surface recombination rates ( $R_l$  and  $R_r$ ), and surface thermal generation rates ( $\mathcal{G}_{lt}$  and  $\mathcal{G}_{rt}$ ), given in (15) should be modified to

$$\begin{aligned} R_l - \mathcal{G}_{lt} &= \hat{\mathcal{K}}_l n^{\alpha-1} p^{\beta-1} (np - N_D^2) \Big|_{x=-b^+/2}, \\ R_r - \mathcal{G}_{rt} &= \hat{\mathcal{K}}_r n^{\gamma-1} p^{\tau-1} (np - N_D^2) \Big|_{x=b^-/2}. \end{aligned} \quad (101)$$

Here the case  $\alpha = \beta = \gamma = \tau = 1$  corresponds to direct bimolecular recombination, *i.e.* the case investigated in the §4.1 and  $\hat{\mathcal{K}}_l$  and  $\hat{\mathcal{K}}_r$  play analogous roles to  $\hat{K}_l$  and  $\hat{K}_r$  in (15) although with different dimensions.

Non-dimensionalising (101) via (20) leads to the following dimensionless conditions on the material interfaces

$$\begin{aligned} J^n \Big|_{x=-1/2^+} &= \delta \mathcal{K}_l n^{\alpha-1} p^{\beta-1} (np - N^2) \Big|_{x=-1/2^+}, \\ (J^n - J) \Big|_{x=1/2^-} &= -\delta \mathcal{K}_r n^{\gamma-1} p^{\tau-1} (np - N^2) \Big|_{x=1/2^-} \end{aligned} \quad (102)$$

$$\text{where } \mathcal{K}_l = \Pi_0^{\alpha+\beta-2} \frac{\hat{\mathcal{K}}_l}{\hat{K}b} \quad \text{and} \quad \mathcal{K}_r = \Pi_0^{\gamma+\tau-2} \frac{\hat{\mathcal{K}}_r}{\hat{K}b}. \quad (103)$$

The solution procedure here is identical to that presented in §4.1 with the exception that  $A$  must be recalculated in terms of the new interface conditions (102). In order to do so we

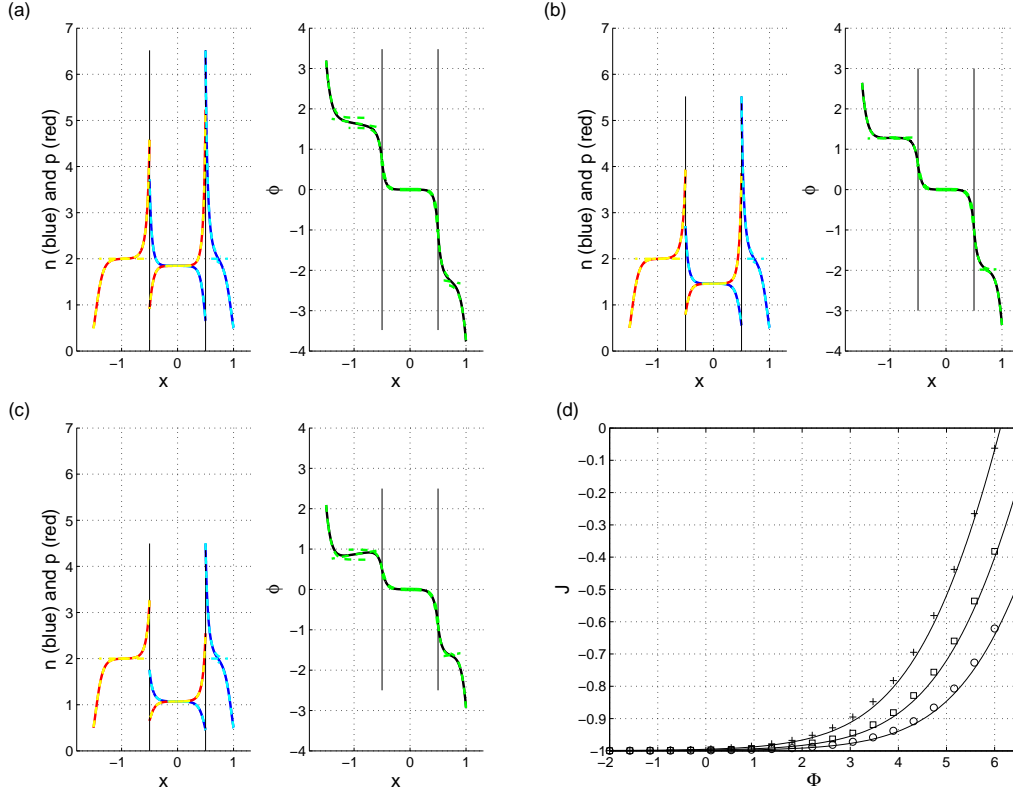


Figure 3: A comparison between the numerical and asymptotic solution of (22)-(29). For the purposes of this demonstration we took the dimensionless parameters to be:  $\int_{x=-1/2}^{x=1/2} G(x)dx = 1$ ,  $\kappa = 1$ ,  $\kappa_n = \kappa_p = 10^2$ ,  $\Lambda_d = \Lambda_a = 1$ ,  $\lambda = 10^{-1}$ ,  $w_d = 1$ ,  $w_a = 0.5$ ,  $\nu_n = 10^{-1}$ ,  $\nu_p = 2 \times 10^{-1}$ ,  $\Phi_{bi} = 0$ ,  $\tilde{N}_- = 1$ ,  $K_l = 0.8$ ,  $K_r = 0.4$ ,  $N = 10^{-1}/\sqrt{2}$  and  $N_a = N_d = 2$ . The panels (a), (b) and (c) were computed with  $\delta = 0.2$  and show the device operating at  $J = 1/2, 0, -1/2$  respectively. Panel (d) shows the current-voltage curve for the same device with  $\delta = 0.2, 0.1, 0.05$  indicated by cross, square and circular markers respectively. A well-documented version of the code used to generated these plots is available in the supplementary material.

insert the asymptotic expression for the electron current in the perovskite (46) into (102), recall that  $B = A$  and substitute for the leading order electron and hole densities on the right and left interfaces, in regions (II) and (V), from (67) (with  $\eta = 0$ ) and (89a-b) (with  $\chi = 0$ ), respectively. This yields the following simultaneous equations for  $A$  and  $h$ :

$$-\frac{\delta(A^2 - N^2) - J}{2} - h + \int_{-1/2}^0 G(x)dx = \mathcal{K}_l \delta A^{\alpha+\beta-2} (A^2 - N^2) \tanh^{2\beta-2\alpha} \left( \sqrt{\frac{A}{2}} \chi_0 \right) \quad (104)$$

$$-\frac{\delta(A^2 - N^2) - J}{2} + h + \int_0^{1/2} G(x)dx = \mathcal{K}_r \delta A^{\gamma+\tau-2} (A^2 - N^2) \tanh^{2\gamma-2\tau} \left( \sqrt{\frac{A}{2}} \eta_0 \right) \quad (105)$$

Summing these two expressions leads to a transcendental equation for  $A$

$$\delta(A^2 - N^2) \left( 1 + \mathcal{K}_l A^{\alpha+\beta-2} g_l(\chi_0) + \mathcal{K}_r A^{\gamma+\tau-2} g_r(\eta_0) \right) = \int_{-1/2}^{1/2} G(x)dx + J, \quad (106)$$

in which  $g_l(\chi_0) = \tanh^{2\beta-2\alpha} \left( \sqrt{\frac{A}{2}} \chi_0 \right)$ ,  $g_r(\eta_0) = \tanh^{2\gamma-2\tau} \left( \sqrt{\frac{A}{2}} \eta_0 \right)$  and  $\eta_0$  and  $\chi_0$  are solutions to (76) and (93), respectively.

#### 4.3.1 The current-voltage curve for non-bimolecular recombination ( $\mathcal{N} \neq 1$ )

In order to obtain the current-voltage relation we must solve for  $\eta_0(A)$  and  $\chi_0(A)$  from (75)-(76) and (92)-(93), substitute the results into (106), solve the resulting equation for  $A$  and insert the resulting functional expression for  $A(J)$  into (98). In practice this requires the use of a numerical root-finding method (we used the 'fsolve' routine in MATLAB with the defaults settings). To summarise the current-voltage curve is given by

$$\Phi \sim \log \left( \frac{A(J)^2}{N^2} \right) + J \left( \frac{w_d}{\kappa N_d} + \frac{w_a \kappa}{N_a} \right) \quad \text{where } A(J) \text{ is determined by the solution to} \quad (107)$$

$$\left\{ \begin{array}{l} \delta(A^2 - N^2) \left( 1 + \mathcal{K}_l A^{\alpha+\beta-2} \tanh^{2\beta-2\alpha} C + \mathcal{K}_r A^{\gamma+\tau-2} \tanh^{2\gamma-2\tau} B \right) = \int_{-1/2}^{1/2} G(x)dx + J, \\ 2\sqrt{\frac{A}{N_a}} = \Lambda_a \sinh(2B) \left( \log \left[ \frac{\nu_n N_a}{A} \coth^2 B \right] - 1 + \frac{A}{\nu_n N_a} \tanh^2 B \right)^{1/2}, \\ 2\sqrt{\frac{A}{N_d}} = \Lambda_d \sinh(2C) \left( \log \left[ \frac{\nu_p N_d}{A} \coth^2 C \right] - 1 + \frac{A}{\nu_p N_d} \tanh^2 C \right)^{1/2}, \end{array} \right. \quad (108)$$

where here we have substituted  $B = \eta_0 \sqrt{A/2}$  and  $C = \chi_0 \sqrt{A/2}$ . In practice, it may be simpler to solve (108b-c) by formulating these two equations in the form of equations for

$\tanh B$  and  $\tanh C$ , respectively. These can be written as

$$\tanh B \sqrt{\left(\frac{A}{\nu_n N_a}\right) \tanh^2 B - 1 + \log\left(\frac{\nu_n N_a}{A \tanh^2 B}\right)} = \frac{(1 - \tanh^2 B)}{\Lambda_a} \sqrt{\frac{A}{N_a}} \quad (109)$$

$$\tanh C \sqrt{\left(\frac{A}{\nu_p N_d}\right) \tanh^2 C - 1 + \log\left(\frac{\nu_p N_d}{A \tanh^2 C}\right)} = \frac{(1 - \tanh^2 C)}{\Lambda_d} \sqrt{\frac{A}{N_d}} \quad (110)$$

**Validity of asymptotics** The calculation of the asymptotic validity of our expansion is more complex than that for bimolecular recombination as a consequence of the complicated relationship between  $A$  and  $J$  given in (108). The result of this calculation is, as before, that  $N \exp(\Phi_{oc}/2)/\lambda^2 \gg 1$ , is a requirement for the results of the asymptotic analysis to be correct over a substantial portion of the current-voltage curve (including the maximum power point).

**Approximations to (107)-(108) for small and large  $A$**  Real current-voltage data of perovskite cells suggests that the potential difference across the cell must reach roughly 1 Volt, corresponding to a dimensionless potential  $\Phi \approx 40$ , before the series resistance term (*i.e.* the second term on the right-hand-side of (107)) becomes appreciable. This corresponds to a change in size of  $A$  on the order of  $e^{20}$ , since  $\Phi$  increases from 0 to 40. We can therefore say a great deal about the nature of the current-voltage relation simply by examining the solutions for  $\tanh B$  and  $\tanh C$  for small and large values of  $A$  and noting that moderate values of  $A$  only occur for a narrow range of the potential  $\Phi$ . We find that

$$\tanh B \rightarrow \left(\frac{\nu_n^{1/2}}{\Lambda_a + \nu_n^{1/2}}\right)^{1/2} \quad \text{and} \quad \tanh C \rightarrow \left(\frac{\nu_p^{1/2}}{\Lambda_d + \nu_p^{1/2}}\right)^{1/2} \quad \text{as} \quad A \rightarrow +\infty \quad (111)$$

$$\tanh B \sim \frac{1}{\Lambda_a} \left(\frac{2}{N_a \log(\nu_n N_a/A)}\right)^{1/2} A^{1/2} \quad \text{for} \quad A \ll 1 \quad (112)$$

$$\tanh C \sim \frac{1}{\Lambda_d} \left(\frac{2}{N_d \log(\nu_p N_d/A)}\right)^{1/2} A^{1/2} \quad \text{for} \quad A \ll 1 \quad (113)$$

It follows that for large  $A$  (107a) is approximated by an algebraic relation for  $A$

$$\left(1 + \mathcal{K}_l \left(\frac{\nu_p^{1/2}}{\Lambda_d + \nu_p^{1/2}}\right)^{\beta-\alpha} A^{\alpha+\beta-2} + \mathcal{K}_r \left(\frac{\nu_n^{1/2}}{\Lambda_a + \nu_n^{1/2}}\right)^{\gamma-\tau} A^{\gamma+\tau-2}\right) \sim \frac{\int_{-1/2}^{1/2} G(x) dx + J}{\delta(A^2 - N^2)} \quad (114)$$

whereas for small  $A$  it is approximated by

$$\left(1 + \mathcal{K}_l \left(\frac{2}{\Lambda_d^2 N_d \log(\nu_p N_d/A)}\right)^{\beta-\alpha} A^{2\beta-2} + \mathcal{K}_r \left(\frac{2}{\Lambda_a^2 N_a \log(\nu_n N_a/A)}\right)^{\gamma-\tau} A^{2\gamma-2}\right) \sim \frac{\int_{-1/2}^{1/2} G(x)dx + J}{\delta(A^2 - N^2)}. \quad (115)$$

We note from (107) that, in the regime where Ohmic losses across the device are insignificant (typically this is true for applied voltages  $\Phi$  less than the open circuit potential  $\Phi_{oc}$ ),  $A \approx N \exp(\Phi/2)$ . Although  $N$ , the ratio of the intrinsic carrier concentration to the typical solar generated carrier concentration, is very small  $\exp(\Phi/2)$  rapidly becomes very large as  $\Phi$  increases from 0 toward around 32 at open circuit.

**An example** Here we illustrate the solution of (107)-(108) with an example in which  $\alpha = 1/4$ ,  $\beta = 5/12$ ,  $\gamma = 1/3$  and  $\tau = 1/6$ . For the purposes of this demonstration we also set the parameters  $\int_{x=-1/2}^{x=1/2} G(x)dx = 1$ ,  $\kappa = 1$ ,  $\kappa_n = \kappa_p = 1/\lambda^2$ ,  $\Lambda_a = \Lambda_d = 1/2$ ,  $w_a = w_d = 1/2$ ,  $\nu_n = \nu_p = 1/4$ ,  $\Phi_{bi} = 0$ ,  $N = 0.1$ ,  $\tilde{N}_- = 1$ ,  $\mathcal{K}_l = 50$ ,  $\mathcal{K}_R = 500$ ,  $N_a = N_d = 4$  and  $\delta = 10^{-5}$  with  $\lambda = 0.05$ . Notably, by plotting  $\log(\int_{-1/2}^{1/2} G(x)dx + J)$  as a function of  $\Phi$  we observe three linear regimes with differing gradients:  $\approx 1$  for small potentials,  $\approx 1/4$  for intermediate potentials and  $\approx 1$  for large potentials; corresponding to idealities  $\mathcal{N} \approx 1$ , 4 and 1 respectively, see figure 4. The model is thus capable of leading to results in which multiple ideality factors are observed in the current-voltage curve.

## 5 Comparison to experiment

The experimentally determined current-voltage relation of a cell constructed using a  $\text{TiO}_2$  acceptor, a lead triiodide perovskite ( $\text{CH}_3\text{NH}_3\text{PbI}_3$ ) and a spiro-OMeTAD donor is shown in figure 5. In panel (b) we plot the variation of  $\log(\int_{x=-b/2}^{x=b/2} G(x)dx + J)$  with  $qV/kT$ . Here, we observe a linear section of the curve (corresponding to the exponential part of the curve in panel (a)) where the device acts like a diode. The gradient of this linear section of curve is a good approximation to the reciprocal of the ideality factor *i.e.*  $1/\mathcal{N}$  [19]. For this cell we find that  $\mathcal{N} \approx 3$  which suggests that recombination in the bulk of the device is relatively unimportant (since it inherently gives rises to an ideality factor  $\mathcal{N} = 1$ ) and instead that the behaviour is largely determined by the recombination at the material interfaces.

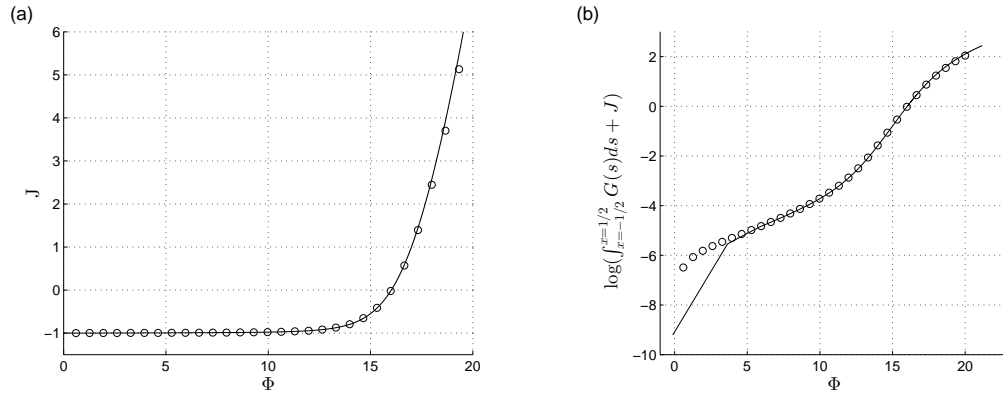


Figure 4: A representative current-voltage relation obtained using the generalised recombination conditions discussed in §4.3 by (i) solving (107)-(108) shown using solid curves, and, (ii) numerical solution of (33)-(35) with the corresponding generalised recombination conditions shown using circular markers. For the purposes of this demonstration we took the dimensionless parameters to be:  $\alpha = 1/4$ ,  $\beta = 5/12$ ,  $\gamma = 1/3$  and  $\tau = 1/6$ ,  $\int_{x=-1/2}^{x=1/2} G(x)dx = 1$ ,  $w_a = w_d = 1/2$ ,  $\Lambda_a = \Lambda_d = 1/2$ ,  $N_a = N_d = 4$ ,  $\nu_n = \nu_p = 1/4$ ,  $N = 0.1$ ,  $\tilde{N}_- = 1$ ,  $\delta = 10^{-5}$ ,  $\mathcal{K}_l = 50$ ,  $\mathcal{K}_R = 500$ ,  $\kappa_n = \kappa_p = 1/\lambda^2$ ,  $\lambda = 0.05$ ,  $\Phi_{bi} = 0$  and  $\kappa = 1$ . In panel (b) we can observe three regimes with differing ideality factors.

This observation motivates us to attempt to reproduce the experimental current-voltage relation by setting  $\alpha = \beta = \gamma = \tau = 1/3$  (so that  $2/(\alpha + \beta) = 2/(\gamma + \tau) = \mathcal{N} = 3$ ) and by taking  $N \ll 1$  and  $\mathcal{K}_l, \mathcal{K}_r \gg 1$  so that the bulk recombination and thermal generation are much less significant than the recombination at the material interfaces. In this case equation (108a) decouples from (108b) and (108c) and has approximate solution (in the limit  $N \rightarrow 0$ ,  $\mathcal{K}_l \gg 1$  and  $\mathcal{K}_r \gg 1$ )

$$A(J) = \left( \frac{\int_{-1/2}^{1/2} G(x) dx + J}{\delta(\mathcal{K}_l + \mathcal{K}_r)} \right)^{3/2}. \quad (116)$$

Inserting this expression into (107) and re-dimensionalising using (20)-(21) gives the following dimensional expression for the current-voltage relation:

$$V = \frac{3kT}{q} \log \left( \frac{q \int_{-b/2}^{b/2} G(x) dx + J}{q N_D^{2/3} (\hat{\mathcal{K}}_l + \hat{\mathcal{K}}_r)} \right) + \frac{kT}{q^2} \left( \frac{d}{\hat{N}_d D_d} + \frac{a}{\hat{N}_a D_a} \right) J. \quad (117)$$

We see from (117) that there are two quantities that determine the shape of the current-voltage curve: (i) the series resistivity integrated over the width of the cell,  $kT(d/\hat{N}_d D_d + a/\hat{N}_a D_a)/q^2$ , and (ii) the reverse saturation current density,  $q N_D^{2/3} (\mathcal{K}_l + \mathcal{K}_r)$ . In the expression for the former the acceptor and donor widths ( $a$  and  $d$ ) and diffusivities ( $D_a$  and  $D_d$ ) are known to reasonable accuracy, however, there is little data on the dopant levels,  $\hat{N}_a$  and  $\hat{N}_d$ . By fitting  $kT(d/\hat{N}_d D_d + a/\hat{N}_a D_a)/q^2$  to the slope of the experimental current voltage curve in the limit  $J \rightarrow \infty$  we can obtain a relation between  $\hat{N}_a$  and  $\hat{N}_d$ . In the expression for the reverse saturation current density,  $q N_D^{2/3} (\mathcal{K}_l + \mathcal{K}_r)$ , we do not have accurate estimates for any of the quantities  $N_D$ ,  $\mathcal{K}_l$  or  $\mathcal{K}_r$ . However by fitting to the experimental current-voltage curve, in the regime in which it grows exponentially, we can obtain an estimate for  $q N_D^{2/3} (\mathcal{K}_l + \mathcal{K}_r)$ . The results of fitting these two quantities to the data yields a very good agreement with the experimental current-voltage curve (see figure 5), and the following estimates:

$$q N_D^{2/3} (\mathcal{K}_l + \mathcal{K}_r) \approx 4.4 \times 10^{-3} \text{ C/m}^2\text{s}, \quad \frac{kT}{q^2} \left( \frac{d}{\hat{N}_d D_d} + \frac{a}{\hat{N}_a D_a} \right) \approx 3.4 \times 10^{-4} \text{ } \Omega\text{m}^2. \quad (118)$$

Due to the lack of existing physical data on perovskite cells it is difficult to say whether or not the first quantity in (118) is reasonable. However, it is noteworthy that on substitution of the known values for  $a$ ,  $d$ ,  $D_a$  and  $D_d$  (shown in table 1) along with  $\hat{N}_a = \hat{N}_d = 10^{24}/\text{m}^3$  (in agreement with the discussion in §1, §2.1.1 and [37]) we arrive at an estimate



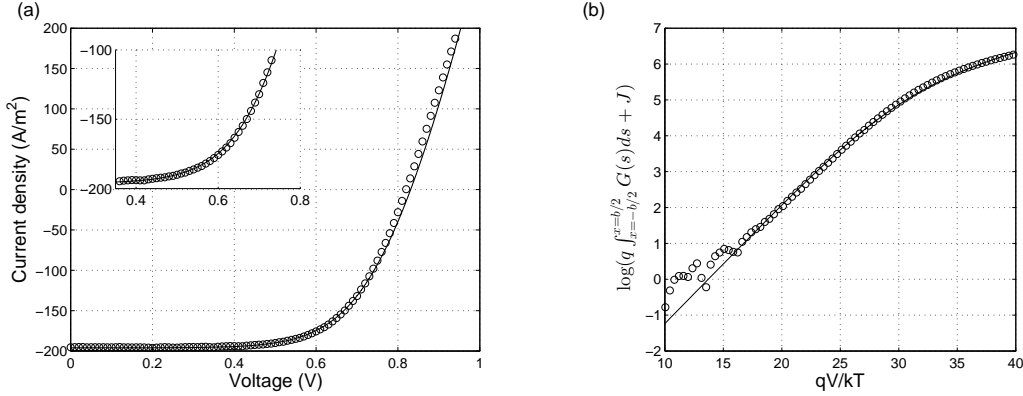


Figure 5: Panels (a) and (b) show an experimental and the fitted asymptotic current-voltage relation. In panel (b) the variation of  $\log(q \int_{x=-b/2}^{x=b/2} G(x) dx + J)$  with  $qV/kT$  so that the gradient of the linear section of the curve is  $1/\mathcal{N} \approx 1/3$ . This experimental data was prepared by Giles Eperon in the Clarendon Laboratory, University of Oxford.

for the series resistivity integrated over the width of the cell that agrees very favourably with the estimate (obtained via fitting) shown in (5.3) - justifying our assumption that the dimensionless dopant densities,  $N_a$  and  $N_d$ , are  $O(1)$ .

## 6 Discussion and conclusions

We have presented a drift-diffusion model for the electrical behaviour of a perovskite based hybrid planar heterojunction solar cell formed from a layer of perovskite sandwiched between layers of acceptor and donor materials that act as selective charge blockers. The basic assumptions of this model are that (i) significant photo-generation occurs only within the perovskite layer, (ii) both acceptor and donor materials are doped, (iii) hole numbers in the acceptor are insignificant, (iv) electron numbers in the donor are insignificant, and (v) electron-hole recombination takes place in the perovskite bulk and on its interfaces with the donor and acceptor. Initially we assumed that recombination (wherever it occurs) is bimolecular and analysed the resulting model in the physically appropriate asymptotic limit in which (I) the charge mobilities in the perovskite layer are much greater than those in the adjacent acceptor and donor layers<sup>3</sup> and (II) the Debye lengths at all four interfaces (contact-donor, donor-perovskite, perovskite-acceptor and acceptor-contact) are much shorter than the widths of the various layers. In this limit we showed that the poten-

<sup>3</sup>This resistance to current flow is dominated by the resistances of the acceptor and donor layers.

tial drop across the device can be divided into (a) drops across the boundary layers at the contacts (which are insensitive to changes in the current flow across the device), (b) drops across the boundary layers at the junctions of the perovskite with the acceptor and the donor (which depend logarithmically on the current flow) and (c) drops across the donor bulk and the acceptor bulk (which both depend linearly on the current flow). This led us to conclude that the current-voltage relationship is asymptotic to that of a Shockley equivalent circuit consisting of a current source in parallel with a diode (ideality factor 1) and in series with a resistor.

However real current-voltage data suggests that the ideality factors of perovskite solar cells are significantly greater than one (and further that they sometimes display more than one ideality factor, *i.e.* the ideality factor can change with the position on the current-voltage curve). This motivated us to consider models for non-bimolecular recombination on the interfaces between the perovskite and the donor, and the perovskite and the acceptor. Here we took the interfacial recombination rates to be given by

$$R_l = \hat{\mathcal{K}}_l n^\alpha p^\beta \quad \text{and} \quad R_r = \hat{\mathcal{K}}_r n^\gamma p^\tau, \quad (119)$$

respectively, where  $n$  and  $p$  denote the electron and hole number densities in the perovskite, on the interface. The main result of the ensuing asymptotic analysis, which is based on the assumptions given above, is the derivation of an asymptotic expression for the current-voltage curve. In its dimensionless form this is given by (107)-(108). On re-dimensionalising this result, via (20) and (103), and on neglecting thermal generation we obtain:

$$\mathcal{A}(J) = N_D \exp \left( \frac{1}{2} \left( \frac{qV}{kT} - \frac{J}{q} \left( \frac{d}{\hat{N}_d D_d} + \frac{a}{\hat{N}_a D_a} \right) \right) \right) \quad \text{where } \mathcal{A}(J) \text{ satisfies (120)}$$

$$\left( \hat{\mathcal{K}} \mathcal{A}^2 + \hat{\mathcal{M}}_l(\mathcal{A}) \mathcal{A}^{\alpha+\beta} + \hat{\mathcal{M}}_r(\mathcal{A}) \mathcal{A}^{\gamma+\tau} \right) = \frac{1}{b} \left( \int_{-b/2}^{b/2} G(x) dx + \frac{J}{q} \right), \quad (121)$$

$$\text{with} \quad \hat{\mathcal{M}}_l(\mathcal{A}) = \hat{\mathcal{K}}_l \tanh^{2\beta-2\alpha} C(\mathcal{A}) \quad \text{and} \quad \hat{\mathcal{M}}_r(\mathcal{A}) = \hat{\mathcal{K}}_r \tanh^{2\gamma-2\tau} B(\mathcal{A}), \quad (122)$$

where  $B(\mathcal{A})$  and  $C(\mathcal{A})$  are calculated from the transcendental equations (108b-c), with  $A = \mathcal{A}/\Pi_0$ . Notably, where each of the interfacial recombination rates are symmetric with respect to holes and electrons (such that  $\beta = \alpha$  and  $\tau = \gamma$ ), the functions  $\hat{\mathcal{M}}_l(\mathcal{A})$  and  $\hat{\mathcal{M}}_r(\mathcal{A})$  are constant and are given by  $\hat{\mathcal{M}}_l(\mathcal{A}) = \hat{\mathcal{K}}_l$  and  $\hat{\mathcal{M}}_r(\mathcal{A}) = \hat{\mathcal{K}}_r$ . In this scenario (121) becomes a simple algebraic equation for  $\mathcal{A}$  in terms of the current density and the generation rate integrated over the width of the perovskite. This can be viewed as an equivalent circuit in which three diodes (with ideality factors 1,  $1/\alpha$  and  $1/\gamma$ ) are in parallel with a current source, and these components are in series with a resistor, see figure 6. In

practical devices the series resistance is insignificant until the applied voltage  $V$  across the device has increased to close to 1 Volt, corresponding to a value of  $qV/kT \approx 40$ . In the range  $0 - 1$  Volt  $\mathcal{A}$  increases by a factor of around  $e^{20}$ . It is therefore possible, depending upon the sizes of the recombination rates, that all three different ideality factors ( $1$ ,  $1/\alpha$  and  $1/\gamma$ ) will be observed, as  $V$  increases, before the series resistance becomes dominant. In cases where there is non-symmetric recombination  $\beta \neq \alpha$  and/or  $\tau \neq \gamma$  an even richer range of behaviour may be observed and this is discussed further in §4.3.1.

In addition to deriving an asymptotic expression for the current-voltage curve we also solved the model numerically and compared these results to the asymptotic solution, both via the predicted current-voltage curves and via the potential and charge carrier density profiles (see figure 3). The agreement we found was extremely good. Finally, in §5, we showed that very good agreement could be obtained between our asymptotic expression for the current-voltage curve and those obtained experimentally.

We remark that the size of the intrinsic carrier density  $N_D$  in the perovskite is unknown and that if it were significantly lower than our estimate that the asymptotic structure of the problem would change. Peltola [32] presents numerical results and detailed discussion of this second scenario showing that charge-carrier depletion occurs in the perovskite layer which, in turn, leads to an increase in its resistance and a large potential drop across the layer. Although the current-voltage predictions here agree marginally better with experimental data than those in [32] there still remains considerable room for doubt about the exact mechanisms underlying the operation of these cells, not least because much of the available current-voltage data is clouded by history effects that arise from long relaxation timescales. Such history effects are currently the subject of much speculation, see [36], being variously ascribed to ferroelectricity in the perovskite, charge-trapping and the slow motion of ions across the cell.

In summary the analysis conducted herein describes the steady-state behaviour of a perovskite solar cell by a relatively simple relation between the current flowing through the cell and the applied voltage (120)-(122). The parameters in this expression depend upon physical properties of the cell, such as recombination rates, charge carrier diffusivities and doping levels. It therefore provides a simple tool for optimising the behaviour of the cell through modifications to its physical properties. An important extension to this work is to investigate the dynamic behaviour of the model. Comparison between time-dependent model results and experimental *transient current decay curves* are expected to lead to further insight into the functioning of the cell.

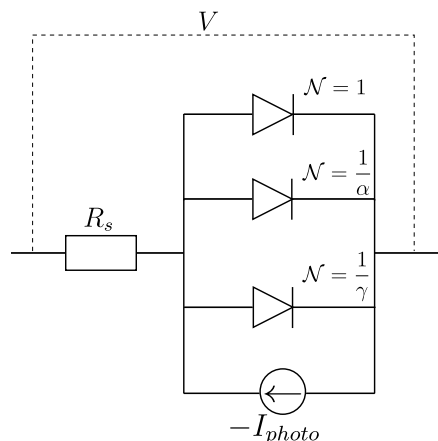


Figure 6: A schematic of the equivalent circuit in the case when each of the interfacial recombination rates are symmetric with respect to electrons and holes, *i.e.* in the case when  $\beta = \alpha$  and  $\tau = \gamma$ . Here,  $I_{photo} = \int_{-b/2}^{b/2} G(x)dx$  and  $R_s = kT/q^2 S \times (d/\hat{N}_d D_d) + (a/\hat{N}_a D_a)$  where  $S$  is the surface area of the cell.

## Acknowledgements

This work was part funded by the EPSRC through grant EP/I01702X/1, and the European Commission, under the SANS project, through grant agreement number 246124. This publication is partially based on work supported by award number KUK-C1-013-04, made by King Abdullah University of Science and Technology (KAUST), via an OCCAM visiting research fellowship awarded to GR. We would also like to thank Colin P. Please for helpful discussions and Giles Eperon who prepared the experimental data discussed in §5.

## References

- [1] M. B. Anderson, M van Soestbergen, A. Mani, H. Bruus, P. M. Biesheuvel & M. Z. Bazant, “Current-induced Membrane Discharge”. *Phys. Rev. Lett.*, **109**: 108301 (2012).
- [2] J. M. Ball, M. M. Lee, A. Hey & H. J. Snaith, “Low-temperature processed meso-structured to thin-film perovskite solar cells”. *Energy Environ. Sci.*, **6**: 1739-1743 (2013).

- [3] Z. Battles & L. N. Trefethen, "An extension of matlab to continuous functions and operators". *SIAM J. Sci. Comput.*, **25**: 1743-1770 (2004).
- [4] M. Z. Bazant, K. T. Chu & B. J. Bayly, "Current-voltage relations for electrochemical thin films". *SIAM J. Appl. Math.*, **65**: 1463-1484 (2005).
- [5] D. Brinkman, K. Fellner, P. A. Markowich & M. T. Wolfram, "A drift-diffusion-reaction model for excitonic photovoltaic bilayers: asymptotic analysis and a 2-D HDG finite-element scheme". *Math. Models and Methods in Appl. Sci.*, **23**: 839-872 (2013).
- [6] G. A. Buxton & N. Clarke, "Modelling the current-voltage characteristics of bilayer polymer photovoltaic devices". *Phys. Rev. B*, **67**: 075205 (2003).
- [7] D. Cheyns, J. Heremans, P. Deibel, C. Verlaak, S. Rand & J. Genoe, "Analytical model for the open-circuit voltage and its associated resistance in organic planar heterojunction solar cells". *Phys. Rev. B*, **77**: 165332 (2008).
- [8] K. T. Chu & M. Z. Bazant, "Electrochemical thin films at and above the classical limiting current". *SIAM J. Appl. Math.*, **65**: 1485-1505 (2005).
- [9] B. K. Crone, P. S. Davids, I. H. Campbell & D. L. Smith, "Device model investigation of bilayer organic light emitting diodes". *J. Appl. Phys.*, **87**: 1974 (2000).
- [10] P.S. Davids, I.H. Campbell & D.L. Smith, "Device model for single carrier organic diodes". *J. Appl. Phys.*, **82**: 6319 (1997).
- [11] T. A. Driscoll, F. Bornemann & L. N. Trefethan, "The Chebop system for automatic solution of differential equations". *BIT Num. Math.*, **48**: 701-723 (2008).
- [12] L. Etgar, P. Gao, Z. Xue, Q. Peng, A. K. Chandiran, B. Liu, Md. K. Nazeeruddin & M. Grätzel, Mesoscopic  $\text{CH}_3\text{NH}_3\text{PbI}_3/\text{TiO}_2$  heterojunction solar cells. *JACS*, **134**: 17396-17399 (2012).
- [13] J. M. Foster, J. Kirkpatrick & G. Richardson, "Asymptotic and numerical prediction of current-voltage curves for an organic bilayer solar cell under varying illumination and comparison to the Shockley equivalent circuit". *J. Appl. Phys.*, **114**: 104501 (2013)
- [14] M. A. Green, K. Emery, Y. Hishikawa, W. Warta & E. D. Dunlop. Solar cell efficiency tables (version 39). *Progress in photovoltaics*, **20**: 12-20 (2011).

- [15] M. A. Green, K. Emery, Y. Hishikawa, W. Warta & E. D. Dunlop. Solar cell efficiency tables (version 40). *Progress in photovoltaics*, **20**: 606-614 (2012).
- [16] K. A. Gregg & M. C. Hanna, “Comparing organic to inorganic photovoltaic cells: Theory, experiment, and simulation”. *J. Appl. Phys*, **93**: 3605-3614 (2003).
- [17] A. Haldi, A. Sharma, W. J. Potscavage, & B. Kippelen, “Origin of the open-circuit voltage in multilayer heterojunction organic solar cells”. *Appl. Phys. Lett.*, **93**: 193308 (2008).
- [18] K. Kamran, M. van Soestbergen, H. P. Huinink & L. Pel, “Inhibition of electrokinetic ion transport in porous materials due to potential drops induced by electrolysis”. *Electrochem. Acta*, **78**: 229-235 (2012).
- [19] A. Jain & A Kapoor. “A new method to determine the diode ideality factor of a real solar cell using the Lambert W-function”. *Sol. Ener. Mat. and Solar Cells.*, **85**: 391-396 (2005).
- [20] P. E. de Jongh & D. Vanmaekelbergh, “Trap-Limited Transport in Assemblies of Nanometer-Size TiO<sub>2</sub> Particles”. *Phys. Rev. Lett.*, **77**: 3427-3430 (1996).
- [21] H. Kim, C. Lee, J. Im, K. Lee, T. Moehl, A. Marchioro, S. Moon, R. Humphry-Baker, J. Yum, J. E. Moser, M. Grätzel & N. Park. “Lead Iodide perovskite sensitized all-solid-state submicron thin film mesoscopic solar cell with efficiency exceeding 9%”. *Sci. rep.*, **2**: 591 (2012).
- [22] R. G. E. Kimber, E. N. Wright, S. E. J. O’Kane & A. B. Walker, “Mesoscopic kinetic Monte Carlo modeling of organic photovoltaic device characteristics”. *Phys. Rev. B* **86**: 235206 (2012).
- [23] T. Kirchartz, B. E. Pieters, J. Kirkpatrick, U. Rau & J. Nelson, “Recombination of tail states in polythiophene: fullerene solar cells”. *Phys. Rev. B.*, **83**:115209 (2011).
- [24] J. Kirkpatrick, V. Marcon, K. Kremer, J. Nelson, D. Andrienko, “Charge mobility in discotic mesophases: a multiscale quantum and classical study”. *Phys. Rev. Lett.*, **98**: 227402 (2007).
- [25] L. J. A. Koster, E. C. P. Smits, V. D. Mihailetschi & P. W. M. Blom, “Device model for the operation of polymer/fullerene bulk heterojunction solar cells”. *Phys. Rev. B.*, **72**: 085205, (2005).

- [26] I. B. Koutselas, L. Ducasse & G. C. Papavassiliou, “Electronic properties of three- and low-dimensional semiconducting materials with Pb halide and Sn halide units”. *J. Phys.: Condens. Matter*, **8**: 1217-1227 (1996).
- [27] M. M. Lee, J. Teuscher, T. Miyasaka, T. N. Murakami & H. J. Snaith, “Efficient hybrid solar cells based on meso-structured organometal halide perovskites”. *Science*, **338**: 634-647 (2012).
- [28] T. Leijtens, J. Lim, J. Teuscher, T. Park & H. J. Snaith, “Charge density dependent mobility of organic hole-transporters and mesoporous TiO<sub>2</sub> determined by transient mobility spectroscopy: Implications to dye-sensitized and organic solar cells”. *Advanced Materials*, **25**: 3227-3233 (2013).
- [29] G. G. Malliaras & J. C. Scott, “The roles of injection and mobility in organic light emitting diodes”. *J. Appl. Phys.*, **83**: 5399-5403 (1998).
- [30] R. E. O’Malley & C. Schmeiser. The asymptotic solution of a semiconductor device problem involving reverse bias. *SIAM J. Appl. Math.*, **50**: 504-520 (1990).
- [31] L. Pautmeier, R. Richert & H. Bässler, “Poole-Frenkel behaviour of Charge Transport in organic solids with off-diagonal disorder studied by Monte Carlo simulation”. *Synth. Met.*, **37**: 271 (1990).
- [32] T. Peltola, "Characterisation of dye-sensitized solar cells for process control". University of Bath PhD Thesis (2014).
- [33] G. Richardson, C. Please, J. M. Foster & J. Kirkpatrick, “Asymptotic solution of a model for bilayer organic diodes and solar cells”. *SIAM J. Appl. Math.*, **72**: 1792-1817 (2012).
- [34] A. Schenk & U. Krumbein, “Coupled defect-level recombination: Theory and application to anomalous diode characteristics”. *J. Appl. Phys.*, **78**: 3185-3192 (1995).
- [35] C. Schmeiser & A. Unterreiter, “The derivation of analytic device models by asymptotic methods”. *Semiconductors, Part II, IMA Vol. in Math. and its Appl.* 59, Springer-Verlag (1993).
- [36] H.J. Snaith, A. Abate, J.M. Ball, G.E. Eperon, T. Leijtens, N.K. Noel, S.D. Stranks, J. T.-W. Wang, K. Wojciechowski & W. Zhang “Anomalous Hysteresis in Perovskite Solar Cells”. *J. Phys. Chem. Lett.*, **5**: 1511-1515 (2014)

- [37] H. J. Snaith Group, unpublished data.
- [38] M. van Soestbergen, P. M. Biesheuvel & M. Z. Bazant, “Diffuse-charge effects on the transient response of electrochemical cells”. *Phys. Rev. E* **81**: 021503 (2010).
- [39] S. M. Sze, K. Ng Kwok, “Physics of Semiconductor Devices”. 3rd edition, Wiley-Interscience NY, (2006).
- [40] L. N. Trefethen & others, “Chebfun Version 4.2”, The Chebfun Development Team, <http://www.maths.ox.ac.uk/chebfun/> (2011).
- [41] W. Tress, K. Leo & M. Riede, “Influence of hole-transport layers and donor materials on open-circuit voltage and shape of I-V curves of organic solar cells”, *Adv. Func. Mater.* **21**: 2140-2149 (2011).
- [42] A. B. Walker, “Monte Carlo studies of electronic processes in dye-sensitized solar cells”, *Topics in Current Chemistry* (2013).
- [43] W. Zhang, M. Saliba, S. D. Stranks, Y. Sun, X. Shi, U. Wiesner & H. J. Snaith, “Enhancement of perovskite-based solar cells employing core-shell metal nanoparticles”, to appear in *Nano Lett.* (2013).

## A Equilibrium solution and derivation of Ohmic boundary conditions

We start by recalling that, where the Fermi Level does not lie within a few  $kT$  of the valence and conduction band edges, the Fermi-Dirac distributions for electron and hole densities in a semiconductor ( $n$  and  $p$ , respectively) can be approximated by

$$n(x) = \bar{g}_c(x) \exp\left(-\frac{E_c(x) - E_f}{kT}\right) \quad \text{and} \quad p(x) = \bar{g}_v(x) \exp\left(-\frac{E_f - E_v(x)}{kT}\right), \quad (123)$$

where  $E_f$  is the Fermi Level,  $E_c(x)$  is the electron energy at the conduction band edge (or LUMO),  $E_v(x)$  is the electron energy at the valence band edge (or HOMO),  $\bar{g}_c(x)$  is the density of states in the conduction band (or LUMO) and  $\bar{g}_v(x)$  is the density of states in the valence band (or HOMO). The spatial dependence of  $E_c$  and  $E_v$  is given in (1). Similarly,  $\bar{g}_c$  and  $\bar{g}_v$  are also piece-wise constant functions that take the following values in each of



the materials:

$$\bar{g}_c(x) = \begin{cases} \hat{g}_c & \text{for } -b/2 < x < b/2, \\ g_c & \text{for } b/2 < x < a + b/2, \end{cases} \quad (124)$$

$$\bar{g}_v(x) = \begin{cases} g_v & \text{for } -d - b/2 < x < -b/2, \\ \hat{g}_v & \text{for } -b/2 < x < b/2. \end{cases} \quad (125)$$

In the metallic cathode the Fermi Level is given by

$$E_f = -q\phi_{cath} - W_{cath} \quad (126)$$

where  $\phi_{cath}$  and  $W_{cath}$  are the potential in the cathode and the work function of the cathode, respectively. Similarly in the anode contact

$$E_f = -q\phi_{anod} - W_{anod} \quad (127)$$

where  $\phi_{anod}$  and  $W_{anod}$  are the potential in the anode and the work function of the anode, respectively. Since the Fermi Level,  $E_f$ , is uniform throughout the device it follows that the built in potential of the cell  $V_{bi}$ , which measures the potential difference between the anode and cathode at equilibrium, is given by

$$V_{bi} = \phi_{anod} - \phi_{cath} = \frac{1}{q}(W_{cath} - W_{anod}). \quad (128)$$

We illustrate the equilibrium configuration of the perovskite solar cell under consideration in figure 7. The various bands indicated in this diagram show the vacuum electron potential (solid red), the electron potential at the conduction band edge (solid green) and the electron potential at the valence band edge (solid purple purple). The spacing between the Fermi Level and the flat sections of the valence and conduction bands, that lie away from interfacial Debye layers, is determined by the doping levels in the semiconductors (thus these are evenly spaced about the Fermi Level in an undoped material, such as the perovskite). Having fixed these bands in relation to the Fermi Level, the energy of the vacuum level can be determined by noting that the gap between the conduction band edge (or LUMO) and the vacuum level is given by the electron affinity of the material whilst that between the valence band edge (or HOMO) and the vacuum level is given by the the ionisation potential of the material. The drop (increase) in the energy of the vacuum level, of size  $-q\phi$ , in the various layers of the device below (above) that of the cathode arises from the potential difference between the material and the cathode. Continuity of the potential (and therefore also the

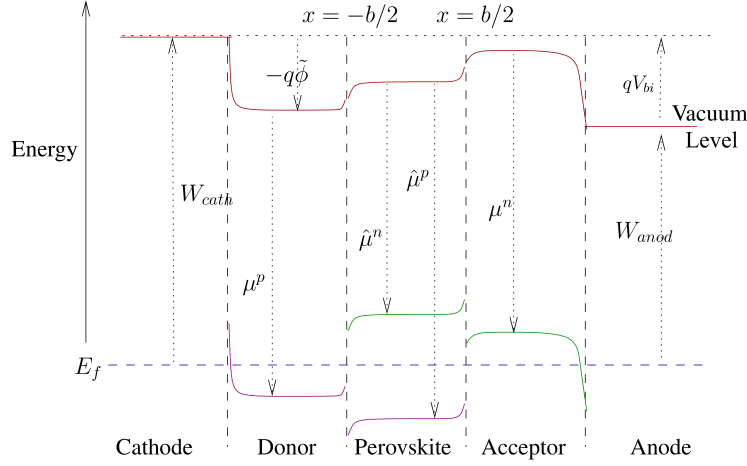


Figure 7: Typical band bending diagram for a planar trilayer perovskite solar cell at equilibrium. Vacuum level indicated by red curves, conduction bands (or LUMOs) by green curves and valence bands (or HOMOs) by purple curves. Here  $\tilde{\phi}$  measures the potential with respect to the cathode. Upward and downward arrows indicate positive and negative quantities, respectively.

vacuum level) forces the bands to bend near the material interfaces across the interfacial Debye layers.

Our aim here is to derive interfacial conditions and boundary conditions, on the dynamic model of the solar cell, that are consistent with the equilibrium solution discussed above. We assume, even where the cell is not in equilibrium, that electron and hole concentrations equilibrate either side of the cathode-donor, donor-perovskite, perovskite-acceptor and acceptor-anode interfaces. Making use of (1) and (123)-(125) we obtain the following conditions for the ratio of hole densities on either side of the donor-perovskite interface

$$\frac{p|_{x=-b/2+}}{p|_{x=-b/2-}} = \frac{\hat{g}_v}{g_v} \exp\left(\frac{\hat{\mu}^p - \mu^p}{kT}\right), \quad (129)$$

and for the ratio of electron densities on either side of perovskite-acceptor interface

$$\frac{n|_{x=b/2-}}{n|_{x=b/2+}} = \frac{\hat{g}_c}{g_c} \exp\left(\frac{\mu^n - \hat{\mu}^n}{kT}\right). \quad (130)$$

In the perovskite the intrinsic carrier density  $N_D$  is defined in terms of the product of the equilibrium values of the two different species of free charge carriers, *i.e.*  $np = N_D^2$ , from

which (and from (123)) it follows that

$$N_D^2 = \hat{g}_c \hat{g}_v \exp\left(\frac{\hat{\mu}^p - \hat{\mu}^n}{kT}\right). \quad (131)$$

While on the two contacts we can use (123)-(127) to show that

$$p|_{x=-(b/2+d)} = g_v \exp\left(\frac{\mu^p + W_{cath}}{kT}\right) \quad \text{and} \quad n|_{x=b/2+a} = g_c \exp\left(-\frac{\mu^n + W_{anod}}{kT}\right) \quad (132)$$

Multiplying the above two conditions and using (128)-(131) to eliminate the term  $g_v g_c \exp((\mu^p - \mu^n + W_{cath} - W_{anode})/(kT))$  we obtain the following global condition relating the interface conditions to the boundary conditions

$$p|_{x=-(b/2+d)} n|_{x=b/2+a} = N_D^2 \exp\left(\frac{qV_{bi}}{kT}\right) \frac{p|_{x=-b/2-} n|_{x=b/2+}}{p|_{x=-b/2+} n|_{x=b/2-}} \quad (133)$$